

# Summertime observations of elevated levels of ultrafine particles in the high Arctic marine boundary layer

Julia Burkart<sup>1</sup>, Megan D. Willis<sup>1</sup>, Heiko Bozem<sup>2</sup>, Jennie L. Thomas<sup>3</sup>, Kathy Law<sup>3</sup>, Peter Hoor<sup>2</sup>, Amir A. Aliabadi<sup>4</sup>, Franziska Köllner<sup>5</sup>, Johannes Schneider<sup>5</sup>, Andreas Herber<sup>6</sup>, Jonathan P. D. Abbatt<sup>1</sup>, W. Richard Leitch<sup>7</sup>.

[1] {Department of Chemistry, University of Toronto, Toronto, Canada}

[2] {Institute of Atmospheric Physics, Johannes Gutenberg-University, Mainz, Germany}

[3] {LATMOS/IPSL, UPMC Univ. Paris 06 Sorbonne Universités, UVSQ, CNRS, Paris, France}

[4] {Environmental Engineering Program, University of Guelph, Guelph, Canada}

[5] {Particle Chemistry Department, Max Planck Institute for Chemistry, Mainz, Germany}

[6] {Alfred Wegener Institute, Helmholtz Center for Polar and Marine Research, Bremerhaven, Germany}

[7] {Environment and Climate Change Canada, Toronto, Ontario, Canada}

Correspondence to: J. Burkart (jburkart@chem.utoronto.ca)

## Abstract

Motivated by increasing levels of open ocean in the Arctic summer and the lack of prior altitude-resolved studies, extensive aerosol measurements were made during 11 flights of the NETCARE July 2014 airborne campaign from Resolute Bay, Nunavut. Flights included vertical profiles (60 to 3000 m above ground level) over open ocean, fast ice, and boundary layer clouds and fogs. A general conclusion, from observations of particle numbers between 5 and 20 nm in diameter ( $N_{5-20}$ ), is that ultrafine particle formation occurs readily in the Canadian high Arctic marine boundary layer, especially just above ocean and clouds, reaching values of a few

26 thousand particles/cm<sup>3</sup>. By contrast ultrafine particle concentrations are very much lower in the  
27 free troposphere. Elevated levels of larger particles (for example, from 20 to 40 nm in size, N<sub>20-</sub>  
28 <sub>40</sub>) are sometimes associated with high N<sub>5-20</sub>, especially over low clouds, suggestive of aerosol  
29 growth. The number densities of particles greater than 40 nm in diameter (N<sub>>40</sub>) are relatively  
30 depleted at the lowest altitudes, indicative of depositional processes that will lower the  
31 condensation sink and promote new particle formation. The number of cloud condensation nuclei  
32 (CCN, measured at 0.6% supersaturation) are positively correlated with the numbers of small  
33 particles (down to roughly 30 nm), indicating that some fraction of these newly formed particles  
34 are capable of being involved in cloud activation. Given that the summertime marine Arctic is a  
35 biologically active region, it is important to better establish the links between emissions from the  
36 ocean and the formation and growth of ultrafine particles within this rapidly changing  
37 environment.

38

## 39 **1 Introduction**

40 Surface temperatures within the Arctic are rising almost twice as fast as in any other region of  
41 the world. As a manifestation of this rapid change the summer sea ice extent has been retreating  
42 dramatically over the past decades with the possibility that the Arctic might be ice free by the  
43 end of this century (Boé et al., 2009) or even earlier (Wang and Overland, 2012). Arctic aerosol  
44 is well known to show a distinct seasonal variation with maximum mass concentrations and a  
45 strong long-range anthropogenic influence in winter and early spring. The phenomenon, known  
46 as Arctic Haze, was identified many years ago (e.g. Barrie, 1986; Heintzenberg, 1980; Rahn et  
47 al., 1977; Shaw, 1995), and has commanded renewed attention in recent years (e.g. Law et al.,  
48 2014; Quinn et al., 2007). During summer the Arctic is more isolated from remote anthropogenic  
49 sources and represents a comparatively pristine environment. The reason is that the Arctic front  
50 (e.g. Barrie, 1986), which provides a meteorological barrier for lower-level air mass exchange,  
51 moves north of many source regions during the summer months. Anthropogenic and biomass  
52 burning aerosols are transported to the Arctic during the summer, but increased aerosol  
53 scavenging helps maintain the pristine conditions near the surface (e.g. Browse et al., 2012; Croft  
54 et al., 2016a; Garrett et al., 2011).

55 Zhang et al. (2010) discuss the impacts of declining sea ice on the marine planktonic ecosystem,  
56 which includes increasing emissions of dimethyl sulfide (DMS) that may contribute to particle  
57 formation in the atmosphere (e.g. Charlson et al., 1987; Pirjola et al., 2000). Enhanced secondary  
58 organic aerosol from emissions of biogenic volatile organic compounds is also a possibility (Fu  
59 et al., 2009). Primary emissions of aerosol particles from the ocean, such as sea salt and marine  
60 primary organic aerosol, may also increase (Browse et al., 2014). Open water tends to increase  
61 cloudiness, which means that aerosol influences on clouds are likely to be more important. Over  
62 the Arctic the effects of aerosols on clouds are especially uncertain. Models have predicted that  
63 increasing numbers of particles may lead to overall warming (Garrett, 2004) when the  
64 atmosphere exists in a particularly low particle number state now referred to being "CCN  
65 limited" (Mauritsen et al., 2011), to an overall cooling effect when increasing numbers of  
66 particles are added to an atmosphere with more particles already present (Lohmann and Feichter,  
67 2005; Twomey, 1974). It is important to characterize particle size distributions in this pristine  
68 environment to provide a baseline against which future measurements can be compared in a  
69 warming world. Indeed, Carslaw et al. (2013) highlight the need to understand pre-industrial-like  
70 environments with only natural aerosols in order to reduce the uncertainty in estimations of the  
71 anthropogenic aerosol radiative forcing.

72 Primary sources, gas-to-particle formation processes, cloud processing, atmospheric aging,  
73 mixing and deposition are all reflected in the size distribution. Therefore, measurements of  
74 aerosol size distributions are important for understanding the processes particles undergo in  
75 addition to their potential effects on clouds. The presence of ultrafine particles indicates recent  
76 production as their lifetime is on the order of hours. We focus this paper on ultrafine particles as  
77 these are an indication for in-situ aerosol production processes in the Arctic. We also consider  
78 the growth of newly formed particles, as that determines how important they are for climate.

79 Aerosol size distributions including ultrafine particles ( $dp < 20$  nm) have been measured before  
80 at different locations throughout the Arctic. Long term studies at ground stations such as Alert,  
81 Nunavut (Leaith et al., 2013), Ny Alesund and Zeppelin (Engvall et al., 2007; Ström et al.,  
82 2003, 2009; Tunved et al., 2013), both on Svalbard and very recently in Tiksi, Russia (Asmi et  
83 al., 2016) and Station Nord, Greenland (Nguyen et al., 2016) indicate a strong seasonal

84 dependence of the size distribution with the accumulation mode aerosol dominating during the  
85 winter months and a shift to smaller particles during the summer months. New particle formation  
86 events are frequently observed from June to August. Ström et al. (2003) show that the size  
87 distribution undergoes a rapid change from an accumulation mode dominated distribution during  
88 the winter months to an Aitken mode dominated distribution at the beginning of summer. Total  
89 number concentrations increase at the beginning of summer and roughly follow the incoming  
90 solar radiation on a seasonal scale suggesting that photochemistry is an important factor for new  
91 particle formation in the Arctic. At Ny Alesund maximum number concentrations occur in late  
92 summer and are explained by the Siberian tundra being a potential source of aerosol precursor  
93 gases (Ström et al., 2003) and marine biogenic sulphur (Heintzenberg and Leck, 1994). Analysis  
94 of air mass patterns for this region show that the shift in the size distributions is also  
95 accompanied by a change of source areas, with a dominance of Eurasian source areas in winter  
96 and North Atlantic air during summer (Tunved et al., 2013).

97 Particle measurements including aerosol size distributions were also conducted from ice breaker  
98 cruises such as from the Swedish ice breaker Oden (Bigg and Leck, 2001; Covert et al., 1996;  
99 Heintzenberg and Leck, 2012; Leck and Bigg, 2005; Tjernström et al., 2014) and the Canadian  
100 Coast Guard Ship ice breaker Amundsen (e.g. Chang et al., 2011). Chang et al. (2011) used  
101 model calculations to show that the appearance of ultrafine particles can be explained by  
102 nucleation and growth attributed to the presence of high atmospheric and oceanic DMS  
103 concentrations measured at the same time. The Oden expeditions focus on the pack-ice-covered  
104 high Arctic, mainly north of 80N and also confirm the frequent presence of an UFP mode (e.g.  
105 Covert et al., 1996). The observations from the Oden cruises offer evidence that UFP in the inner  
106 Arctic might originate from primary sources (e.g. Heintzenberg et al., 2015; Karl et al., 2013).  
107 This is motivated by three main observations. First, a lack of sulfuric acid components in  
108 collected 15-50 nm particles (Leck and Bigg, 1999). Second, Leck and Bigg (2010) highlight  
109 that nucleation events in the high Arctic do not follow the classical banana shaped growth curve  
110 (Kulmala et al., 2001) but enhanced levels of ultrafine particles rather appear simultaneously in  
111 distinct size ranges (Karl et al., 2012). Third, such events could not be modelled with the selected  
112 empirical nucleation mechanism for the extremely low DMS concentrations in this region (Karl

113 et al., 2013). As a primary source marine microgels are suggested that might become airborne via  
114 the evaporation of fog and cloud droplets (Heintzenberg et al., 2006; Karl et al., 2013).

115 So far most studies that include size distribution measurements in the summertime Arctic were  
116 conducted from ground stations or ship cruises. To date there are only two studies that assess the  
117 altitude dependence of the size distribution:, i.e. one in the area of Svalbard (Engvall et al., 2008)  
118 and one from the Oden performing vertical profiles with a helicopter (Kupiszewski et al., 2013).  
119 Although no size distribution measurements were performed, Heintzenberg et al. (1991)  
120 measured vertical profiles of the total particle number concentration greater than 10 nm during  
121 June and July, 1984 over the Fram Strait-Spitsbergen area, and found a “rather uniform  
122 distribution” with altitude. Their measurements, however, were confined to 500 m-MSL and  
123 above.

124 In this study we present data from aerosol size distribution measurements taken from an aircraft  
125 during a three week period in July 2014 in the high Arctic area of Resolute Bay, Nunavut,  
126 Canada. The flights focused on vertical profiles from as low as 60 m above the ground up to  
127 3km, as well as on low-level flights above different terrain such as fast ice, open ocean, polynyas  
128 and clouds. We focus especially on UFP (5-20 nm in diameter) and address the following  
129 questions: What are the concentrations of UFPs in the Arctic summertime, and what is their  
130 vertical distribution? What are the environmental conditions that favour occurrence of UFPs?  
131 And, is there evidence for growth of UFP to CCN sizes? Aside from the studies conducted near  
132 Svalbard, we believe this is the first aircraft study in the high Arctic to systematically address  
133 these specific questions. This work provides a comprehensive picture of UFPs observed during  
134 the campaign whereas a prior publication from Willis et al., (2016) detailed one UFP formation  
135 and growth event observed over Lancaster Sound.

136

## 137 **2 Experimental**

### 138 **2.1 Sampling Platform Polar 6**

139 The research aircraft Polar 6 owned by the Alfred Wegener Institute, Helmholtz Center for Polar  
140 and Marine Research, Bremerhaven, Germany served as the sampling platform. The Polar 6 is a

141 converted DC-3 airplane (Basler BT-67) modified to work under extreme cold weather  
142 conditions. An advantage of the plane is that flights at very relatively low speeds and altitudes  
143 (< 60 m a.g.l.) are possible. The cabin of the aircraft is non-pressurized. We maintained a  
144 constant survey speed of approximately 120 knots (222 km h<sup>-1</sup>) for measurement flights at  
145 constant altitude, and ascent and descent rates of 150 m min<sup>-1</sup> for vertical profiles. Instruments  
146 and measurements specific to this paper are described below.

### 147 2.1.1 Inlets

148 Aerosol was sampled through a stainless steel inlet mounted to the top of the plane and ahead of  
149 the engines to exclude contamination. The tip of the inlet consisted of a shrouded diffuser that  
150 provided nearly isokinetic flow. Inside the cabin the intake tubing was connected to a stainless  
151 steel tube (outer diameter of 2.5 cm, inner diameter of 2.3 cm) that carried the aerosol to the back  
152 of the aircraft where it was allowed to freely exhaust into the cabin so that the system was not  
153 over-pressured. The stainless steel tube functioned as a manifold, off which angled inserts were  
154 used to connect sample lines to the various instruments described below. In-flight air was pushed  
155 through the line with a flow rate of approximately 55 L min<sup>-1</sup> determined by the sum of the flows  
156 drawn by the instruments (35 L min<sup>-1</sup>), plus the flow measured at the exhaust of the sampling  
157 manifold (20 L min<sup>-1</sup>). A flow of 55 L min<sup>-1</sup> was estimated to meet nearly isokinetic sampling  
158 criteria at survey speed and the transmission of particles through the main inlet was  
159 approximately unity for diameters between 20 nm to 1 μm (Leitch et al., 2016). Although the  
160 transfer of the aerosol from outside to the instruments is relatively fast (5 seconds or less),  
161 volatilization of some components of the particles may have occurred. However, the growth of  
162 newly formed particles by organic condensation occurs primarily by low volatility organic  
163 components (e.g. Pierce et al., 2012). Thus, the integrity of the smaller particles is likely to have  
164 been maintained. We do expect increasing line losses of particles with sizes decreasing from 10  
165 nm. Therefore our observations will underestimate N<sub>5-20</sub>.

166 Trace gases (CO and H<sub>2</sub>O) were sampled through a separate inlet made of a 0.4 cm (outer  
167 diameter) Teflon tube entering the aircraft at the main inlet and exiting through a rear-facing 0.95  
168 cm exhaust line that provided a lower line pressure. The sample flow of approximately 12 L min<sup>-1</sup>  
169 <sup>1</sup> was continuously monitored.

## 170 **2.2 Instrumentation**

### 171 2.2.1 Meteorological parameters and state parameters

172 Aircraft state parameters and meteorological measurements were performed with an AIMMS-20  
173 manufactured by Aventechn Research Inc. at a very high sampling frequency ( $>40\text{Hz}$ ). The  
174 AIMMS-20 consists of three modules: (1) The Air Data Probe that measures the three-  
175 dimensional aircraft-relative flow vector (true air speed, angle-of-attack, and sideslip), and  
176 turbulence with a three-dimensional accelerometer. As well, temperature and humidity sensors  
177 are contained within this unit and provide an accuracy and resolution of 0.30 and 0.01 C for  
178 temperature and 2.0 and 0.1% for relative humidity measurements. (2) An Inertial Measurement  
179 Unit that consists of three gyros and three accelerometers providing the aircraft angular rate and  
180 acceleration; (4) A Global Positioning System for aircraft 3D position and inertial velocity.  
181 Horizontal and vertical wind speeds were measured with accuracies of 0.50 and 0.75  $\text{m s}^{-1}$ ,  
182 respectively. The high frequency raw data were processed to 1Hz resolution. Further details of  
183 the AIMMS including data processing can be found in (Aliabadi et al., 2016a).

### 184 2.2.2 Aerosol physical and chemical properties

185 Particle number concentrations and particle size distributions were measured with a TSI 3787  
186 water-based ultrafine Condensation Particle Counter (UCPC), a Droplet Measurement  
187 Technology (DMT) Ultra High Sensitivity Aerosol Spectrometer (UHSAS) and a Brechtel  
188 Manufacturing Incorporated (BMI) Scanning Mobility System (SMS) coupled with a TSI 3010  
189 Condensation Particle Counter (CPC). The UCPC detected particle concentrations of particles  
190 larger than 5nm in diameter with a time resolution of 1 Hz. The flow rate was set to 0.6  $\text{L min}^{-1}$ .  
191 The particle concentrations measured by the UCPC are referred to as  $N_{\text{tot}}$  hereafter, noting as  
192 above that diffusional losses of particles smaller than 10 nm make the  $N_{\text{tot}}$  observations lower  
193 limits.

194 The BMI SMS was set to measure particle size distributions from 20nm to 100nm with a sample  
195 flow of 1  $\text{L min}^{-1}$  and a sheath flow of 6  $\text{L min}^{-1}$ . The duration of one scan was 40 s with a 20 s  
196 delay time before each scan resulting in a time resolution of 1min. The UHSAS performed size  
197 distribution measurements from 70 nm – 1  $\mu\text{m}$  at a time resolution of 1 Hz with a sample flow

198 rate of  $55 \text{ cm}^3 \text{ min}^{-1}$ . Details of the calibrations and instrument inter-comparisons performed  
199 prior and during the campaign are described in detail in Leaitch et al. (2016).

200 Cloud condensation nuclei (CCN) were measured with a DMT CCN Counter (CCNC). The  
201 CCNC was operated behind a constant pressure inlet that was set to 650 hPa. The nominal  
202 supersaturation was held constant at 1%. Calibrations prior and during the campaign (for details  
203 see Leaitch et al. 2016) showed that a nominal supersaturation of 1% at the reduced pressure  
204 translated into 0.6% effective supersaturation.

205 Cloud droplet sizes from 2-45  $\mu\text{m}$  were measured using a wing mounted Particle Measuring  
206 System (PMS) FSSP 100. In this study these data are only used to identify periods when the  
207 aircraft was flying in cloud. To avoid possible artefacts produced from shattering of cloud  
208 droplets at the aerosol inlet, data from in-cloud times are discarded for the purposes of this study.

209 A DMT Single Particle Soot Photometer (SP2) was deployed to measure refractory black carbon  
210 (rBC) number and mass concentrations. We refer to rBC mass concentrations as an indication of  
211 pollution influence. Calibrations with Aquadag soot were performed prior to and during the  
212 campaign. The lower size limit of detection of rBC particles by the SP2 was approximately  
213 80nm.

214 Sub-micron aerosol composition was measured with an Aerodyne high-resolution time-of-flight  
215 aerosol mass spectrometer (HR-ToF-AMS; e.g. DeCarlo et al., 2006). A detailed description of  
216 the instrument is found in Willis et al. 2016. The main purpose of the instrument was to measure  
217 non-refractory particulate matter such as sulfate, nitrate, ammonium, methane sulfonic acid  
218 (MSA) and the sum of organics. Detection limits were 0.009, 0.008, 0.004, 0.005 and  $0.08 \mu\text{g m}^{-3}$ ,  
219 respectively, for a 30 second averaging time.

220

### 221 2.2.3 Trace gases

222 Carbon monoxide (CO) was measured with an Aerolaser ultra-fast carbon monoxide monitor  
223 model AL 5002 based on VUV fluorimetry, employing the excitation of CO at 150 nm. In-situ  
224 calibrations were performed during flight at regular intervals (15 – 30 min) using a NIST



225 traceable CO standard with zero water vapor concentration. CO mixing ratios were used as a  
226 relative indicator of aerosol influenced by pollution sources.

227 Water vapour (H<sub>2</sub>O) measurements were based on infrared absorption using a LI-7200 enclosed  
228 CO<sub>2</sub>/H<sub>2</sub>O Analyzer from LI-COR Biosciences GmbH. The measurement uncertainty is ± 15  
229 ppm<sub>v</sub>. H<sub>2</sub>O mixing ratios were used to calculate relative humidity with pressure and temperature  
230 measured by the AIMMS-20.

### 231 **2.3 Data analysis and nomenclature of particle size data**

232 All particle data were averaged to 1 min intervals to match the time resolution of the BMI SMS.  
233 Particle concentrations within different size intervals were calculated. The notation N<sub>a-b</sub> is used;  
234 “a” gives the lower limit and “b” the upper limit of the calculated size interval. The BMI SMS  
235 was used to determine concentrations of particles from 20-90 nm diameter, and concentrations of  
236 particles larger than 90 nm diameter were determined by the UHSAS. If the size interval is  
237 expressed as N<sub>>a</sub> the upper limit is given by the detection limit of the UHSAS (1µm).  
238 Additionally, particle concentrations from 5-20 nm (short: N<sub>5-20</sub>) were obtained by subtracting  
239 particle concentrations measured by the BMI SMS and by the UHSAS from the N<sub>tot</sub> as  
240 determined by the CPC. The N<sub>5-20</sub> are also referred to as ultrafine particles (UFP) in this study  
241 and may be indicative of newly formed particles. Willis et al. (2016) showed that for this  
242 environment particles were able to grow to 50 nm low over the open water over approximately  
243 one hour, which means that the growth from 1 nm to 10 nm can occur over approximately one  
244 minute or less, justifying our use of instruments that are sensitive to 5 nm particles and larger.  
245 For the concentration range of N<sub>5-20</sub> particles (less than 2000 cm<sup>-3</sup>), it requires more than 30  
246 hours for the concentration of 10 nm particles to be reduced by coagulation to a concentration of  
247 500 cm<sup>-3</sup> (Agranovski 2010).

248 In order to obtain vertical profiles the data were averaged within altitude intervals. An average  
249 profile for a single flight was obtained by binning all data from the respective flight into altitude  
250 intervals of 100m starting at the lowest flight altitude. In addition to data obtained during vertical  
251 profile flights, data acquired while flying at a constant level were also included. Average profiles

252 containing data from more than one flight were calculated by averaging the respective single  
253 flight profiles.

254 Average size distributions were obtained by simply averaging each bin for the desired time and  
255 altitude range. The size distributions measured by the BMI SMS were used for particle sizes  
256 from 20-90 nm, and the distributions at larger sizes are taken from the UHSAS. All particle  
257 concentrations are expressed for ambient pressure conditions, i.e. they have not been adjusted to  
258 standard temperature and pressure conditions. The  $N_{5-20}$  referred to as UFP are added to the size  
259 distributions as additional bin assuming a bin width of 15 nm (from 5-20 nm) with the mid  
260 diameter of 12nm.

261

## 262 **2.4 FLEXPART-WRF Simulations**

263 We used FLEXPART-WRF (Brioude et al., 2013, website: [flexpart.eu/wiki/FpLimitedareaWrf](http://flexpart.eu/wiki/FpLimitedareaWrf))  
264 simulations run backwards in time to analyse the origins of air masses sampled along the flight  
265 tracks. FLEXPART-WRF is a Lagrangian particle dispersion model based on FLEXPART (Stohl  
266 et al., 2005). Meteorological information is obtained from the Weather Research and Forecasting  
267 (WRF) Model (Skamarock et al., 2005). FLEXPART-WRF outputs retroplume information such  
268 as the residence time of air (over a unit area) prior to sampling. Residence times were integrated  
269 over the entire atmospheric column and 7 days backward in time. FLEXPART-WRF was run in  
270 two ways. First, one FLEXPART-WRF was completed for each flight using particle releases  
271 every 2 minutes along the flight track (100 m x 100 m x 100 m centered on the aircraft location)  
272 to produce potential emissions sensitivities (PES) that represent the average air mass origin for  
273 each flight. Second, separate runs were completed for points (every 10 minutes) along the flight  
274 track (100 m x 100 m x 100 m, 60 second release duration) in order to study different air masses  
275 measured during the same flight. A more detailed description of the model as used for  
276 NETCARE 2014 is provided by Wentworth et al. (2015).

277

## 278 **2.5 Study area and flight tracks**

279 From July 4<sup>th</sup> to July 21<sup>st</sup>, 2014 eleven flights were conducted out of Resolute Bay (74.7 N, 95.0  
280 W). In Figure 1 a compilation of all flight tracks on a satellite image is shown. The satellite  
281 picture was taken on July 4<sup>th</sup>, 2014 and reflects the situation of the region during period I (July 4  
282 to July 12). Resolute Bay proved to be an ideal location for this study as we had access to both  
283 open ocean and ice covered regions. Additionally two polynyas were located north of Resolute  
284 Bay within the reach of our aircraft. Flights ranged between 4-6 hours. The flights covered two  
285 main areas: Lancaster Sound east of Resolute Bay and the area north of Resolute Bay where two  
286 polynyas were located. The flights south of Resolute Bay in Lancaster Sound concentrated  
287 around the ice edge.

288 The ice/water coverage visible on the satellite picture is representative for the area during the  
289 first period. As can be seen, the ice edge was situated about 150 km east of Resolute Bay. It is  
290 clearly visible in the satellite image as a sharp line. The transition from a completely ice covered  
291 region to open ocean was very abrupt during the first period. Only after a period of bad weather  
292 with high winds did the ice edge become less clear, and the region starting about 80 km east of  
293 Resolute Bay to about 200 km east was covered by fractured ice.

294 Roughly 50% of the flight time was within the inversion layer, and 50% was in the free  
295 troposphere conducting altitude profile flights. A considerable amount of time was spent at 2800  
296 m as this was the preferred altitude when travelling to a certain area. When clouds were present,  
297 the aircraft sampled them by slant profiling through the cloud in the case clouds were above the  
298 boundary layer, or, in the case clouds were within 200 m of the surface, by descending into the  
299 cloud as low as possible. Aerosol observations while inside cloud are excluded from the analysis  
300 here due to potential artifacts from droplets shattering on the outside inlet.

301

## 302 **3 Meteorological and atmospheric conditions**

303 Meteorological conditions changed over the course of the campaign. Similar conditions were  
304 encountered during the first part of the campaign (July 4<sup>th</sup> – July 12<sup>th</sup>, 6 flights), referred to as the  
305 “Arctic air mass period” because air masses from within the Arctic dominated and the

306 atmosphere showed structures typical for the Arctic such as a low boundary layer height with  
307 thermally stable conditions, indicated by a near surface temperature inversion, and frequent  
308 formation of low level clouds. At this time Resolute Bay was under the influence of high  
309 pressure systems. Clear sky with few or scattered clouds and low wind speeds dominated.  
310 Conditions changed starting from July 13<sup>th</sup> when the region was influenced by troughs of a low  
311 pressure system located to the west above Beaufort Sea, which eventually passed through  
312 Resolute Bay on July 15<sup>th</sup> bringing along humidity, precipitation and fog. Intense fog and low  
313 visibility impeded flying from July 13<sup>th</sup> to July 16<sup>th</sup>. A short good weather window in which the  
314 fog dissipated permitted flying again on July 17<sup>th</sup> (referred to as “transition day”; one flight) just  
315 before Resolute Bay came under influence of a pronounced low pressure system located to the  
316 south with its center around King William Island (69.0 N, 97.6 W). The last campaign days  
317 (referred to as “southern air mass period”, three flights) were characterised by the influence of  
318 this pronounced low pressure system bringing air masses from the south and providing higher  
319 wind speeds, an overcast sky and occasional precipitation.

320

321 Vertical profiles of median temperature, relative humidity (RH), wind speed, CO and  $N_{\text{tot}}$  (Figure  
322 2) illustrate median atmospheric conditions during the measurement flights. Prominent features  
323 representing the trend of each period and reflecting the general meteorological situation will be  
324 described here, with details discussed in the respective sections. The Arctic air mass period was  
325 characterized by frequent thermally stable conditions within the near surface layer, representing  
326 typical conditions during the Arctic summertime (Aliabadi et al., 2016a; Tjernström et al., 2012).  
327 The median temperature profiles show that on average the boundary layer reached up to ~300 m  
328 with a temperature increase of about 5 C. In this paper we will refer to this part of the  
329 atmosphere as the boundary layer (BL) and to the air masses above as the free troposphere (FT).  
330 A BL height of 300m corresponds well to the boundary layer height of 275 +/- 164 m estimated  
331 by (Aliabadi et al., 2016a) using the method of bulk Richardson number (Aliabadi et al., 2016b)  
332 and a critical bulk Richardson number of 0.5, using data from radiosondes launched at Resolute  
333 Bay and the Amundsen icebreaker, which also performed research operations in Lancaster sound  
334 during the campaign period.

335 Within the BL particle concentrations spanned over a wide range of concentrations (max  $N_{\text{tot}}$ :  
336  $\sim 10000$ ; median values:  $\sim 150$  to  $\sim 1700 \text{ cm}^{-3}$ ). Highest  $N_{\text{tot}}$  occurred during the Arctic air mass  
337 period, while  $N_{\text{tot}}$  was constantly low within the lower atmosphere on the transition day. Median  
338 temperatures near the surface ranged from  $-1 \text{ C}$  to  $5 \text{ C}$  during the Arctic air mass period, largely  
339 depending on the terrain below (e.g. ice or open water) and were clearly higher during when the  
340 southern air masses arrived (e.g. at the “surface”:  $4 \text{ C}$  and  $7 \text{ C}$ , respectively) and, if present, the  
341 BL was less pronounced. The higher temperatures coincide with the influence of low pressure  
342 systems bringing warmer air masses from the west and south and additional higher wind speeds  
343 providing a better mixing of the atmospheric layers ( $5.6 \text{ ms}^{-1}$  vs  $12 \text{ m}^{-1}$  near the surface). CO  
344 mixing ratios were extremely low during the Arctic air mass period (median:  $78.3 \text{ ppb}_v$ ) and on  
345 the transition day (median:  $83.4 \text{ ppb}_v$ ) indicating pristine air masses that had not recently been  
346 affected by pollution or biomass burning sources. During the southern air mass influence CO  
347 mixing ratios clearly increased (median:  $95.0 \text{ ppb}_v$ ) confirming a change in air mass and  
348 suggesting possible influences by pollution sources and wild fires in the North West Territories  
349 (Supplementary Figure 2). Relative humidity profiles show that the near surface layer of the  
350 atmosphere was very moist with  $\text{RH} > 80 \%$  during all periods.

351

## 352 **4 Results and Discussion**

### 353 **4.1 Ultrafine particle events**

#### 354 **4.1.1 Frequency of ultrafine particle events**

355 Throughout the campaign we observed large variability in particle concentrations (Figure 3). We  
356 observed not only very clean air masses with  $N_{\text{tot}}$  of a few tens  $\text{cm}^{-3}$  (with the lowest 1-second  
357 value of  $1 \text{ cm}^{-3}$ ), but also concentrations as high as a few thousands per  $\text{cm}^{-3}$  (with the highest  
358 value of  $10000 \text{ cm}^{-3}$ ). The highest and lowest concentrations were measured within the BL  
359 (Figure 3b). Above the BL (Figure 3b) particle concentrations were relatively constant where  
360 60% of the time concentrations were between  $200 - 300 \text{ cm}^{-3}$  (for a discussion of the average size  
361 distribution see sections 4.1.2 - 4.1.4). Especially during the Arctic air mass period (Figure 2) the  
362 atmosphere was characterized by a strong contrast between the BL and the FT.

363 UFP were very frequently present within the BL in high concentrations (Figure 3c). Here we  
364 refer to "bursts" of particles as a sudden and relatively large increase in  $N_{5-20}$ : concentrations  
365 suddenly rising from tens  $\text{cm}^{-3}$  to several hundreds and thousands  $\text{cm}^{-3}$ . This may reflect  
366 inhomogeneities in the NPF process or reflect the aircraft flying in and out of areas of high UFP  
367 concentrations. Bursts of  $N_{5-20} > 2000/\text{cm}^3$  were observed over polynyas, consistent with  
368 previous observations (Leaitch et al., 1984; 1994), in Lancaster Sound and south of Resolute  
369 Bay. The  $N_{5-20}$  was higher than  $200 \text{ cm}^{-3}$  during 65% of the time. Indeed, high  $N_{\text{tot}}$  was mainly  
370 driven by UFP (as can be seen by comparison of black dots indicating high  $N_{\text{tot}}$  in Figure 3c and  
371 high UFP in Figure 3d). Whenever  $N_{\text{tot}}$  is greater than  $2000 \text{ cm}^{-3}$ , UFP was larger than  $1000 \text{ cm}^{-3}$ .  
372 This is also illustrated by the ratio of  $\text{UFP}/N_{\text{tot}}$  (Figure 3e). A ratio of zero means that no UFP  
373 were present, while a ratio of one means that only UFP were present. Within the boundary layer  
374 32% of the time the size distribution was dominated by UFP (ratio  $> 0.5$ ).

375 The frequent presence of UFP agrees well with other studies made during the Arctic summertime  
376 at several locations, such as at the ground stations in Ny Alesund and Zeppelin (Ström et al.,  
377 2009; Tunved et al., 2013), at Alert (Leaitch et al., 2013), and from ship-based observations  
378 (Chang et al., 2011; Covert et al., 1996; Heintzenberg et al., 2006). However, such a frequent  
379 presence of an UFP mode (65% of the time  $> 200 \text{ cm}^{-3}$ ) in the BL is unique to this study.  
380 Possible reasons for the higher occurrence of UFP might be the combination of the proximity of  
381 open ocean (providing a source of UFP or precursor gases), favourable meteorological  
382 conditions (sunny weather, inversion layer with cloud formation) and very clean air masses with  
383 low condensation sinks. Also, since observations of UFP were one focus of this study, the  
384 fractional occurrence of the UFP mode may be biased slightly high due to longer sampling times  
385 associated with UFP occurrence. Calm weather conditions may have been another factor. The  
386 highest concentrations of UFP were measured at lower wind speeds ( $< 5 \text{ m s}^{-1}$ ; Supplementary  
387 Figure 1), while lower UFP concentrations ( $1000 \text{ cm}^{-3}$ ) were found at higher wind speeds  
388 ( $> 12 \text{ m s}^{-1}$ ) suggesting a dilution effect of the wind. Such a dilution effect implies proximity to the  
389 source.

390 In the following sections, the vertical distribution of UFP and the size distributions are discussed  
391 in relation to meteorological conditions during the three distinct periods that characterized this  
392 campaign.

393

#### 394 4.1.2 Arctic air mass period: July 4<sup>th</sup> to July 12<sup>th</sup>

395 During this first period the study area was under the influence of a high pressure system. As  
396 illustrated by FLEXPART-WRF results (Figure 4a and 4b), air masses were either coming from  
397 the North extending to the east in the Arctic Ocean or from the East passing over the open ocean  
398 in Lancaster Sound and Baffin Bay. Both examples indicate that air masses resided within the  
399 Arctic region at least 5 days prior to sampling. This is true for all flights during this period. The  
400 very low CO mixing ratios (78 ppb<sub>v</sub>, see Figure 2) and average BC mass concentrations of 3 ng  
401 m<sup>-3</sup> (not shown) confirm that air masses were very clean and without recent influence from  
402 pollution sources. As discussed in section 3, temperature profiles indicate thermally stable  
403 conditions in the lowest layers with near-surface temperature inversions. During almost all  
404 vertical profiles we observed temperature inversions of about 4-6 C near the surface. Such an  
405 atmospheric structure i.e. a shallow boundary layer is typical for the Arctic summertime (e.g.  
406 Aliabadi et al., 2016a; Tjernström et al., 2012).

407 The Arctic air mass period was characterized by a very sharp contrast between the BL and the  
408 FT in terms of particle number concentrations and sizes (Figure 5). The BL was characterized by  
409 a prominent layer of UFP from the surface to about 300 m with the highest concentrations closest  
410 to the surface (Figure 5a). The height of the UFP layer coincides with the average height of the  
411 temperature inversion for this period (see temperature profile Figure 2) and indicates that air  
412 masses were stably layered limiting exchange with the FT. This is supported by the observed  
413 lower turbulent mixing (i.e. turbulent kinetic energy) from boundary layer to the free troposphere  
414 during the campaign (Aliabadi et al., 2016a).

415 During this period we measured the highest concentrations of UFPs with the one minute average  
416 up to 5300 cm<sup>-3</sup>. On a typical flight several bursts (see Section 4.1.1) of high UFP concentrations  
417 were encountered in the BL. Particle bursts lasted from a few seconds to several minutes,

418 corresponding to a spatial extent of several hundreds of meters to dozens of kilometers. The large  
419 spatial variability is also illustrated by the frequency distribution of UFP in the BL shown in  
420 Figure 5c: 40% of the time concentrations of UFP were larger than  $200 \text{ cm}^{-3}$ , 11% of the time  
421 larger than  $1000 \text{ cm}^{-3}$  and 3% of the time even larger than  $2000 \text{ cm}^{-3}$ . Particle concentrations in  
422 the FT are relatively uniform, and concentrations of UFP were less than  $50 \text{ cm}^{-3}$  up to 1200m and  
423  $\sim 10 \text{ cm}^{-3}$  above.

424 The average  $N_{20-40}$  is similar to the UFP, showing a maximum in its concentration at the same  
425 altitude. The concentrations of larger particles ( $N_{>40}$ ,  $N_{>80}$ ,  $N_{>150}$ ) are much lower in the clean BL  
426 (surface areas of  $\sim 5 \mu\text{m}^2 \text{ m}^{-3}$  and lower). However, the  $N_{>40}$  and  $N_{>80}$  increase from the lowest  
427 altitude to the next averaged altitude, consistent with the increase in the UFP and  $N_{20-40}$ . These  
428 results suggest that some of the UFP experienced growth to sizes of 20-80 nm within a few  
429 hours, as demonstrated by Willis et al. (2016). Within the FT particle concentrations were  
430 surprisingly uniform and concentrations of UFP were less than  $50 \text{ cm}^{-3}$  up to 1200m and  $\sim 10 \text{ cm}^{-3}$   
431 above.

432 In Figure 5b, the median size distribution shows that increases in UFP in the BL were frequent.  
433 The average size distribution shows that at times higher concentrations of particles extended up  
434 to about 80 nm, consistent with the suggestion above that some UFP particles experienced  
435 growth to larger sizes. A relevant case will be discussed in Section 4.3. Occasionally a mode of  
436 particles larger than 400 nm was present in the BL over open water (see Section 4.2), which was  
437 likely the product of primary oceanic emissions.

438

#### 439 4.1.3 Transition day on July 17<sup>th</sup>

440 July 17th marks the transition from dominance by Arctic air masses to a more distant influence  
441 from southern air masses. The transition day consists of only one flight in the area of Lancaster  
442 Sound, during which low concentrations of particles larger than 20 nm were observed below 600  
443 m: e.g.  $N_{>40}$  ranged from  $60 \text{ cm}^{-3}$  to  $100 \text{ cm}^{-3}$ ; see Figure 6. The deeper layer of lower  
444 concentrations may have been a result of cloud processing and scavenging. During the days  
445 before flying was impossible because of intense fog and cloud at Resolute Bay. A different



446 transport regime may also have contributed to this situation. On this day the low pressure system  
447 situated to the west was bringing air masses from the west along the Canadian and Alaskan  
448 coastline (Figure 4c). The temperature profile shows an inversion between 650-1000m possibly  
449 indicating a change in air mass. CO mixing ratios (83ppb<sub>v</sub>) and BC mass concentrations (3ng/cm<sup>3</sup>)  
450 were also quite low indicating mostly Arctic background conditions.

451 On this day, occasional bursts of UFP up to 1400-1900 cm<sup>-3</sup> were observed within the boundary  
452 layer (Figure 6b). UFP of 200 cm<sup>-3</sup> or more were observed about 20% of the time (Figure 6c),  
453 and the average concentration was 240 cm<sup>-3</sup> at the lowest level of the profile (Fig. 6a).  
454 Concentrations of larger particles (N<sub>>40</sub>, N<sub>>80</sub>, N<sub>>150</sub>) increased sharply at about 700m coinciding  
455 with the temperature inversion. The very low concentrations of larger particles (N<sub>>150</sub>: <10 cm<sup>-3</sup>)  
456 below the temperature inversion are very similar to the conditions encountered within the BL  
457 during the previous period. As above, the differences in the transition day below 700 m may  
458 have been due to a combination of fog/cloud scavenging and a change of air mass. Median and  
459 average size distributions indicate a minimum at around 65nm that might be the result of cloud  
460 processing (Hoppel et al., 1994), consistent with the Arctic observations of (Heintzenberg et al.,  
461 2006) and the activation diameters observed during this study (Leaitch et al., 2016).

#### 462 4.1.4 Southern air mass period: July 19<sup>th</sup> – July 21<sup>st</sup>

463 During this period the region was under the influence of a low pressure system centered south of  
464 Resolute Bay. FLEXPART-WRF air mass trajectories (Figures 4d and 4e) indicate a prevalence  
465 of air masses from the south potentially affected by wild fires (see Supplementary Figure 2). At  
466 the beginning of this period on July 19<sup>th</sup> (Figure 4d), air mass trajectories suggest the strongest  
467 influence from the south while towards the end of the period on July 21<sup>st</sup> (Figure 4e),  
468 FLEXPART-WRF indicates that southern air masses mixed with air masses coming off  
469 Greenland. Near surface temperatures were higher than during the previous periods (Figure 2)  
470 and temperature inversions were less pronounced (2-4 C) and not observed at all locations  
471 suggesting a less stable lower atmosphere. On July 19<sup>th</sup> we encountered the highest wind speeds  
472 in the BL (16 m/s within the near surface layer and 20 m/s slightly above). Also RH was  
473 relatively high near the surface (91%) and did not drop below 80% throughout the vertical

474 atmosphere. CO mixing ratios were higher than during the prior periods suggesting that the air  
475 was at times influenced by pollution or biomass burning.

476 UFP were observed less frequently than during the Arctic air mass period and in lower  
477 concentrations (Figure 7). Bursts of UFP above  $1000 \text{ cm}^{-3}$  occurred only at three locations, all  
478 during the flight on July 21<sup>st</sup>. Average UFP concentrations were only approximately  $190 \text{ cm}^{-3}$ .  
479 UFP concentrations of  $200 \text{ cm}^{-3}$  or higher were detected 31% of the time below 300m (Figure  
480 7c).

481 The southern air mass period clearly shows different aerosol characteristics within the near  
482 surface layer than compared to the Arctic air mass period and the transition day. Average  
483 concentrations of particles larger than 40 nm were highest within the boundary layer and  
484 decreased with altitude (Figure 7a). This is in sharp contrast to the cleaner boundary layers  
485 observed before. Whereas concentrations of particles larger 40nm were  $\sim 100 \text{ cm}^{-3}$  and lower  
486 during both prior periods, they were as high as  $300 \text{ cm}^{-3}$  for this period. Even large accumulation  
487 mode particles ( $N_{>150}$ ) averaged  $\sim 50 \text{ cm}^{-3}$  (compared to  $10 \text{ cm}^{-3}$  for both previous periods). Also,  
488 both the median and average size distributions show a pronounced mode of particles larger than  
489 500 nm within the BL (Figure 7b). Primary emissions from the sea spray promoted by the higher  
490 surface wind speeds (see Figure 2) are likely a factor contributing to the larger particles.

491 During the southern air mass period, three important factors had changed compared to both prior  
492 periods. (1) Air mass back trajectories had clearly shifted to the south and potentially transported  
493 emissions from wild fires located in the Northwest Territories (Supplementary Figure 2) into the  
494 region, which might mix into the boundary layer. (2) The Amundsen ice breaker was present in  
495 Lancaster Sound and acted as a local pollution source. (3) Wind speeds were higher and the  
496 ocean was visibly turbulent with breaking waves that might enhance primary oceanic aerosol  
497 emissions. The increased condensation sinks from these potential sources in combination with  
498 other factors (e.g. reduced sun light) and relatively low residence times of air masses within the  
499 boundary layer (compared to the Arctic air mass period) may explain the relatively low and  
500 infrequent concentrations of UFPs.

501 Within the FT the size distributions shows a bimodal character with a minima at 60-80 nm,  
502 which may indicate the air masses experienced cloud processing. This is likely, given the

503 presence of the low pressure system bringing moister and warmer air masses. The bimodal size  
504 distribution is different from the average size distribution during the Arctic air mass period when  
505 drier air masses from within the Arctic dominated.

## 506 **4.2 UFP occurrence above ice versus water**

507 We investigated the potential influence of different underlying water surfaces on the occurrence  
508 of UFP by examining in detail the time periods when we were flying at altitudes at or below 500  
509 m during the Arctic air mass period. We distinguish between three water surfaces: ice covered  
510 areas (including ice edge and ice covered with melt ponds), open ocean (including polynyas),  
511 and low-level clouds (including both cloud above water and cloud above ice). Here we point out  
512 that the case “cloud” does not include in-cloud flight times but only flight periods when above  
513 cloud top without actually entering the cloud (confirmed by a zero signal in a liquid cloud probe  
514 (FSSP100)). An altitude of 500 m was chosen to include time periods when we were flying  
515 above low-level clouds and to capture mostly flights within the boundary layer where a local  
516 influence of the terrain below was likely. During the Arctic air mass period, there was a clear  
517 separation between ice and open water over Lancaster Sound with east of the ice edge  
518 completely ice free, while west of the ice edge the ocean was seamlessly covered by fast ice (see  
519 satellite picture in Figure 1).

520 Each average profile above the different water surface exhibits unique features (Figure 8). Above  
521 ice the highest concentrations of UFP (average:  $400 \text{ cm}^{-3}$ ) were found nearer the surface (70 m)  
522 and the  $N_{\text{tot}}$  are slightly higher (580). In the BL over open water, the  $N_{\text{tot}}$  and UFP number  
523 concentrations are  $900 \text{ cm}^{-3}$  and  $560 \text{ cm}^{-3}$ , respectively, and in the air just above cloud, the  
524 average  $N_{\text{tot}}$  and UFP number concentrations are  $2000 \text{ cm}^{-3}$  and  $1040 \text{ cm}^{-3}$ , respectively. In the  
525 open water and cloud cases, the highest concentrations of ultrafines are at the point of  
526 measurement closest to the water surface. In the cloud case and open water case, the  $N_{20-40}$   
527 particles show an increase at the same time as the  $N_{\text{tot}}$  and UFP suggesting that the UFP form and  
528 grow to larger sizes. This is not observed in the over-ice case, which suggests that some of the  
529 new particles could have formed elsewhere (e.g. over open water) and been transported over the  
530 ice, or that the growth rates over ice are slow. In all three cases, the largest particles show

531 relatively smaller abundances at the lowest altitudes samples. An increased abundance of UFP at  
532 lower surface areas supports the hypothesis that UFP form via nucleation of precursor gases.

### 533 **4.3 Case study: July 8**

534 The flight on July 8 provides a case study illustrating that the occurrence of UFP is confined to  
535 the BL suggesting a surface source of UFP and that the appearance of UFP is promoted by cloud.  
536 We consider the altitude dependence of the UFP within the BL in relation to air mass history and  
537 cloud.

538 On this flight we first flew out into Lancaster Sound west of Resolute Bay, turned around and  
539 descended into the BL above the ice. Here, we focus on the time period from 15:50 UTC  
540 (descent into the BL) to 17:20 UTC where we travelled from west to east and remained within  
541 the BL but stayed out of cloud as shown in Figure 9; see also Supplementary Figure 2. The later  
542 part of the flight focused on in-situ cloud properties and is discussed elsewhere (Leaitch et al.,  
543 2016). The weather was sunny with low level clouds starting around 150 km over ice and west of  
544 the ice edge in Lancaster Sound. The clouds had formed over the water and were blown over the  
545 ice where they were dissipating (Leaitch et al., 2016). In the entire area the atmosphere was  
546 characterized by a surface temperature inversion extending vertically up to about 300 m with ~1  
547 C near the surface and ~5 C at 300 m and was accompanied by decreasing relative humidity  
548 (Figure 9f). Local low-level winds were predominantly from the south to east and wind speeds  
549 were below 5 ms<sup>-1</sup>.

550 UFP were present throughout the BL with the highest concentrations at the lowest altitudes and  
551 decreasing concentrations towards the top of the BL (Figure 9b). In contrast, larger particles (e.g.  
552 N<sub>>40</sub>) exhibit the opposite pattern, with lower concentrations at lower altitudes and higher  
553 concentrations at higher altitudes. Six locations from west to east (points A-F in Figure 9a) are  
554 used to illustrate the changing aerosol characteristics. Location A is situated well above the BL  
555 and at this point no UFP were present (detailed size distributions are shown in Supplementary  
556 Figure 4). At location B, the point at which we first entered the BL, an UFP mode (~370 cm<sup>-3</sup>)  
557 was present at 60m, while UFP concentrations were lower at slightly higher altitudes (~80 cm<sup>-3</sup>  
558 at 230 m) such as location C. At the lower altitudes the UFP concentrations gradually increased

559 as we approached the ice edge. The most striking observation is the steep increase in particle  
560 concentrations at about 60 km west of the ice edge (location D) where UFP increased to above  
561  $4000 \text{ cm}^{-3}$  at 150 m or just above cloud top. At the same time  $N_{20-40}$  concentrations showed a  
562 similar increase. The increased UFP concentrations were vertically limited to near cloud top and  
563 decreased rapidly with increasing altitude. The same pattern is also observed for temperature,  
564  $\text{H}_2\text{O}$  and  $\text{CO}_2$  (Figure 9g) suggesting the existence of a distinct air mass at the surface that gets  
565 diluted into the air mass above. Further east the flight was restricted to a slightly higher altitude  
566 above cloud top. At point F, where we were close to the BL top, no peaks in particle  
567 concentrations were observed. At point E, just before the ice edge, between the top of cloud and  
568 the top of the BL, UFP concentrations reached about  $3400 \text{ cm}^{-3}$ .

569 Air mass histories at these locations determined from FLEXPART-WRF (Figure 10) indicate the  
570 following:

571 (1) To the west of Resolute Bay (point B) Lancaster Sound air masses had been mixed with air  
572 masses from the North. This is also confirmed by the local wind directions indicating winds  
573 coming from the Northwest sector (Figure 10a), and it is consistent with the associated change in  
574 cloud. (2) Near the top of the BL, air masses had descended recently ( $< 3 \text{ h}$ ) into the BL (Figure  
575 10c point C and point F). (3) In contrast, deeper within the BL at points B and D air masses had  
576 descended into the BL earlier ( $\sim 20 \text{ h}$ ) before arriving at the point of observation. In the case of  
577 point D, where we observed the largest mode of UFP extending above 40nm, air masses had  
578 been travelling from the east exclusively over the open waters in Lancaster Sound during the last  
579 day before arriving at the point of observation.

580 Aerosol composition shows a clear difference between the aerosol in the FT and the BL. The  
581 aerosol sulphate rapidly decreases as we enter the BL around 16:00, while aerosol organic mass  
582 concentrations show an initial relative increase followed by an absolute increase towards the east  
583 (Figure 9c). Within the BL aerosol organics and sulphate mass loadings show a pattern similar to  
584  $N_{>40}$  and  $N_{>80}$ . Both decrease each time we descended deeper into the BL. However, at the same  
585 time the organics-to-sulphate ratio indicates that the relative contribution of organics to aerosol  
586 mass increases at lower altitudes and especially above cloud (Figure 9e). Well within the  
587 inversion layer and in the vicinity of cloud top the aerosol was dominated by organics. At the

588 same time also ratio of MSA to sulphate was higher (Figure 9e), suggesting a marine biogenic  
589 influence of the aerosol sulphur. The marine biogenic influence at the lower altitudes agrees well  
590 with the FLEXPART-WRF simulations showing that air masses at this altitude had spent almost  
591 an entire day exposed to the open waters in Lancaster Sound. Consistent with the higher organic  
592 content measured with the AMS, the single particle aerosol mass spectrometer ALABAMA  
593 (Brands et al., 2011; Willis et al., 2016) detected a higher fraction of trimethylamine (TMA)-  
594 containing particles for particles larger than 150 nm in diameter (F. Köllner, personal  
595 communication, July 2016). Gaseous TMA emissions from marine biogenic origin (Ge et al.,  
596 2011; Gibb et al., 1999) may have additionally favored the subsequent growth of the freshly  
597 nucleated particles by condensation. Another possibility may be uptake of TMA in the cloud  
598 phase (Rehbein et al., 2011) if the particles have grown to sufficiently large sizes to be activated  
599 as CCN. Interestingly, compared to other days these TMA-containing particles are smaller and to  
600 a lesser degree internally mixed with potassium and levoglucosan which supports the hypothesis  
601 of ultrafine particles originating from nucleation in a biogenic marine environment and  
602 subsequent growth.

603 To explain these observations, we hypothesize that the smaller particle mode is formed by  
604 nucleation and growth occurring within the BL and especially in cloud vicinity. UFP  
605 concentrations near cloud top have been reported before (e.g. Radke and Hobbs 1991,  
606 Wiedensohler et al. 1997, Clarke et al., 1999; Garrett et al., 2002; Hegg et al., 1990; Mauldin et  
607 al., 1997) and it is suggested that nucleation in near cloud regions is favoured by the low surface  
608 areas, possibly due to cloud scavenged aerosol, moist air and a high actinic flux. Indeed, near  
609 cloud top where we observed an increase of UFP extending up to almost 50 nm the conditions  
610 for nucleation and growth are ideal. We speculate that the availability of precursor gases is  
611 provided by the long residence time (~20h) of the air masses over open water (Figure 10, point  
612 D). In other words, precipitating clouds scavenge aerosol particles, reducing the surface area for  
613 condensation, but some fraction of nucleation precursor gases with lower Henry's Law constants  
614 can pass through (e.g. SO<sub>2</sub>) leaving the potential for H<sub>2</sub>SO<sub>4</sub> in the higher OH in the cloud  
615 outflow (a discussion of the processes can be found in Seinfeld and Pandis, 1998). The very high  
616 organic loadings and MSA to sulphate ratio likely indicate that the formation and growth of these  
617 particles is driven by a combination of DMS and organic precursors (volatile organic

618 compounds) that are emitted by the open ocean in Lancaster Sound (e.g. Chang et al., 2011;  
619 Sjostedt et al., 2012; Mungall et al., 2016).

620 The event at point E occurs where the aircraft was between cloud top and the top of the BL,  
621 where no increases in UFP were observed before or after. It may be that the aircraft descended  
622 slightly but sufficiently into the cloud-influenced area, which looks to be 25-40 m above cloud  
623 top (Figure 9g), but also at that point we were in vicinity of Prince Leopold Island which is a bird  
624 sanctuary and many bird colonies nest at the 260m high cliff. FLEXPART-WRF and the in-situ  
625 wind measurement show that air masses to a large extent were directly coming off the island  
626 (Figure 10, point E) suggesting a connection between the appearance of UFP and possible  
627 emissions from the fauna of the island. The increase of particle phase ammonium (Figure 9d) at  
628 the same time supports this connection and nucleation of particles from biogenic precursors  
629 emitted by bird colonies are documented (Weber et al., 1998; Wentworth et al., 2016, Croft et al.  
630 2016b).

631 Alternatively, it should be considered that evaporating fog and cloud droplets may also act as a  
632 primary source of UFP (e.g. Heintzenberg et al., 2006; Karl et al., 2013; Leck and Bigg, 1999).  
633 Karl et al., (2013) suggested a combined pathway that involves the emission of UFP by fog and  
634 cloud droplets, together with secondary processes enabling growth of these particles. For our  
635 observations we have no reason to assume that nucleation does not occur since conditions are  
636 ideal but we cannot rule out that nanoparticles are emitted by the possibly evaporating cloud  
637 droplets onto which gases then condense.

638 In conclusion the aerosol mass within the near surface layer is dominated by organics relative to  
639 sulphate, while at just slightly higher altitude sulphate is clearly increased and increases further  
640 above the inversion layer. A high organic content coincides with increases in UFP particles,  
641 especially at times when also growth into the size range up to 50nm is indicated. Similarly the  
642 MSA-to-sulphate ratio shows a peak at the lowest altitudes with maximum values in the vicinity  
643 of clouds that coincide with a long residence time (~20h) of the air masses within the BL and  
644 above open water. The data thereby suggest a marine biogenic influence of the aerosol within the  
645 lower layers of the atmosphere. We note that similarly high levels of aerosol organics and MSA

646 were observed during the flight on July 12 associated with a NPF event and growth but in cloud-  
647 free conditions Willis et al. (2016).

#### 648 **4.4 CCN activity**

649 CCN concentrations were measured at a supersaturation of 0.6%. The vertical profiles of CCN  
650 concentrations (Figure 11a) show patterns similar to those of larger particles. In the very clean  
651 boundary layer of the Arctic air mass period and the transition day CCN concentrations are  
652 equally low ( $\sim 70 \text{ cm}^{-3}$  and  $\sim 50 \text{ cm}^{-3}$ , respectively). In contrast, southern air mass period average  
653 BL CCN concentrations are amongst the highest observed during this campaign ( $>300 \text{ cm}^{-3}$ ).  
654 Within the free troposphere CCN concentrations are surprisingly constant during the Arctic air  
655 mass period ( $120 \pm 27 \text{ cm}^{-3}$ ) and more variable on the transition day ( $92 \pm 46 \text{ cm}^{-3}$ ) and the  
656 southern air mass period ( $103 \pm 67 \text{ cm}^{-3}$ ). The constant CCN concentrations during the Arctic air  
657 mass period correspond to the very uniform atmosphere dominated by aged aerosols we  
658 observed during this period and to the more layered atmosphere influenced by southern air  
659 masses possibly contaminated by biomass burning plumes during the later period. Correlations  
660 with  $N_{>80}$  (Figure 11b) confirm that larger particles are a good approximation for these CCN  
661 concentrations. On average CCN concentrations agree to within  $\pm 20 \%$  of  $N_{>80}$ . However, it  
662 should be noted that slight differences between the 3 periods are indicated in the correlation  
663 curves: during the Arctic air mass period the average activation diameters are smaller than 80  
664 nm, and during the southern air mass period they are larger than 80 nm. Assuming uniform  
665 chemical composition throughout the particle size range, an activation diameter of 80 nm at 0.6%  
666 supersaturation indicates an aerosol much less hygroscopic than, for example, ammonium  
667 sulphate; pure ammonium sulphate particles would activate at 40 nm at 0.6% supersaturation. For  
668 the one specific event during which growth occurred (Willis et al., 2016), it was demonstrated  
669 that high CCN concentrations coincide with elevated organic mass loading. The reduced  
670 hygroscopicity of organic material relative to soluble inorganic salts (Petters and Kreidenweis,  
671 2007) can explain the larger effective activation diameter.

672 A central question is whether and to what degree the CCN are influenced by the UFP. Two  
673 factors help with addressing this question: 1) particles as small as 20 nm and in general much



674 smaller than the average 80 nm size associated with the CCN at 0.6% will nucleate cloud  
675 droplets in the clean environment of the summer Arctic (Leaitch et al., 2016); 2) there is  
676 evidence here that increases in particles larger than 20 nm are associated with increases in the  
677 UFP, particularly for UFP influenced by cloud (e.g. Figure 8). Figure 12 shows regressions of  
678 CCN with UFP,  $N_{>20}$ ,  $N_{>30}$ ,  $N_{>40}$  and  $N_{>50}$ . The high variability in the UFP and the time needed  
679 for a UFP particle to grow to an average size of 80 nm under these low precursor levels does not  
680 permit a direct connection of the CCN and UFP, but in all other cases, the main clusters of the  
681 regressions show quite similar and strong connections with the CCN measurements.  
682 Associations of the UFP with the  $N_{>20}$  in the BL mean that some of these UFP are able to  
683 contribute to cloud-nucleating particles.

684

## 685 **5 Discussion and Conclusions**

686 This study presents airborne observations of ultrafine particles (UFP) during the Arctic  
687 summertime. Eleven flights were conducted in July 2014 in the area of Resolute Bay situated in  
688 the Canadian Archipelago. The location allowed access to open water, ice-covered regions and  
689 low clouds. Flights focused around the ice edge in Lancaster Sound including open waters to the  
690 east, the ice-covered region to the west, and polynas north of Resolute Bay. UFP were observed  
691 within all regions and above all terrains with the highest concentrations encountered in the  
692 boundary layer immediately above cloud and open water. It is shown that UFP occur most  
693 frequently (>65 % of the time) and with the highest concentrations (up to  $5300 \text{ cm}^{-3}$ ) during an  
694 Arctic air mass period when the air is very clean and the boundary layer is thermally stable.

695 The frequent presence of UFP in the boundary layer over open water and low cloud and the  
696 enhanced number concentrations at the lowest altitudes sampled indicate a surface source, such  
697 as the ocean, for the UFP gaseous precursors. This is especially true during the Arctic air mass  
698 period when the sampling region was pristine and not influenced by pollution. FLEXPART-  
699 WRF simulations indicate that air masses had resided within the Arctic region at least 5-7 days  
700 prior to sampling. During this time UFP were restricted to the boundary layer and no UFP events  
701 were observed aloft, thereby excluding that these UFP form in the free troposphere and subside  
702 into the near surface layer e.g. (Clarke et al., 1998; Quinn and Bates, 2011). At the same time we

703 observed an extremely clean boundary layer (surface area of  $N_{>40} \sim 5 \mu\text{m}^2\text{m}^{-3}$ ). Low surface areas  
704 increase the probability of particle formation via nucleation by reducing the surfaces for  
705 precursor gases to condense on.

706 Chlorophyll-a concentrations (Supplementary Figure 5) indicate a relatively high level of  
707 biological activity of the ocean (such as phytoplankton blooms known to produce DMS)  
708 throughout Lancaster Sound, to the east in Baffin Bay and in the open waters of the polynyas  
709 during the time period of the study. Indeed, measurements in Lancaster Sound performed from  
710 the Amundsen ice breaker just a few days after the aircraft campaign show that gas-phase DMS  
711 mixing ratios were high in the Lancaster Sound region (Mungall et al., 2016), up to 1155 ppt<sub>v</sub>.  
712 DMS was also measured from the Polar 6 aircraft with an offline technique. Maximum mixing  
713 ratios of 110 ppt<sub>v</sub> were detected in the surface layer (R. Ghahremaninezhad; personal  
714 communication), again confirming a marine influence in the boundary layer. The measured DMS  
715 concentrations are above the nucleation threshold obtained by modelling performed in the study  
716 of Chang et al. (2011) who concluded that DMS mixing ratios of  $\geq 100\text{ppt}_v$  are sufficient to  
717 account for the formation of hundreds of UFP when background particle concentrations are low.

718 Relating observations of UFP to the surface below during the Arctic air mass period revealed  
719 that the highest UFP concentrations occurred above low-level cloud and open water with  
720 averages of  $1040 \text{ cm}^{-3}$  and  $560 \text{ cm}^{-3}$ , respectively. Above low-level cloud  $N_{20-40}$  showed  
721 increased concentrations. This simultaneous increase in concentrations suggests that UFP grow  
722 into the 40 nm size range, where they can nucleate cloud droplets.

723 Overall, the summertime Arctic is an active region in terms of new particle formation,  
724 occasionally accompanied by growth. The value of these altitude profiles across a wide spatial  
725 extent, performed for the first time in this campaign, is that they demonstrate that this activity is  
726 largely confined to the boundary layer, and that the dominant source of small particles to the  
727 boundary layer does not arise by mixing from aloft but most likely from marine sources. For  
728 future studies, the relative impact of such natural sources of UFP needs to be evaluated with  
729 respect to potential new sources, such as may arise with increasing shipping.

730

731 **Acknowledgements**

732 The authors would like to thank a large number of people for their contributions to this work. We  
733 thank Kenn Borek Air, in particular the pilots Kevin Elke and John Bayes and the aircraft  
734 engineer Kevin Riehl. We are grateful to John Ford, David Heath and the University of Toronto  
735 machine shop for safely mounting our instruments on racks for aircraft deployment. We thank  
736 Jim Hodgson and Lake Central Air Services in Muskoka, Jim Watson (Scale Modelbuilders,  
737 Inc.), Julia Binder and Martin Gerhmann (Alfred Wegener Institute, Helmholtz Center for Polar  
738 Marine Research, AWI), Mike Harwood and Andrew Elford (Environment and Climate Change  
739 Canada, ECCC), for their support of the integration of the instrumentation and aircraft. We  
740 gratefully acknowledge Carrie Taylor (ECCC), Bob Christensen (U of T), Lukas Kandora,  
741 Manuel Sellmann and Jens Herrmann (AWI), Desiree Toom, Sangeeta Sharma, Dan Veber,  
742 Andrew Platt, Anne Marie Macdonald, Ralf Staebler and Maurice Watt (ECCC) for their support  
743 of the study. We thank the Biogeochemistry department of MPIC for providing the CO  
744 instrument and Dieter Scharffe for his support during the preparation phase of the campaign. The  
745 authors J.L. Thomas and K.S. Law acknowledge funding support from the European Union  
746 under Grant Agreement n\_ 5265863 – ACCESS (Arctic Climate Change, Economy and Society)  
747 project (2012-2015) and TOTAL SA. Computer simulations were performed on the IPSL  
748 mesoscale computer center (Mésocentre IPSL), which includes support for calculations and data  
749 storage facilities. We thank the Nunavut Research Institute and the Nunavut Impact Review  
750 Board for licensing the study. Logistical support in Resolute Bay was provided by the Polar  
751 Continental Shelf Project (PCSP) of Natural Resources Canada under PCSP Field Project  
752 #218614, and we are particularly grateful to Tim McCagherty and Jodi MacGregor of the PCSP.  
753 Funding for this work was provided by the Natural Sciences and Engineering Research Council  
754 of Canada through the NETCARE project of the Climate Change and Atmospheric Research  
755 Program, the Alfred Wegener Institute, Helmholtz Center for Polar and Marine Research and  
756 Environment and Climate Change Canada.

757

757 **References**

758 Agranovski, I. (Ed.). *Aerosols: Science and Technology*. 1<sup>st</sup> edition. WILEY-VCH Verlag  
759 GmbH & Co. KGaA, Weinheim, 2010.

760 Aliabadi, A. A., Staebler, R. M., Liu, M. and Herber, A.: Characterization and Parametrization of  
761 Reynolds Stress and Turbulent Heat Flux in the Stably-Stratified Lower Arctic Troposphere  
762 Using Aircraft Measurements, *Boundary-Layer Meteorol.*, doi:10.1007/s10546-016-0164-7,  
763 2016a.

764 Aliabadi, A. A., Staebler, R. M., de Grandpré, J., Zadra, A. and Vaillancourt, P. A.: Comparison  
765 of Estimated Atmospheric Boundary Layer Mixing Height in the Arctic and Southern Great  
766 Plains under Statically Stable Conditions: Experimental and Numerical Aspects, *Atmosphere-*  
767 *Ocean*, 54(1), 60–74, doi:10.1080/07055900.2015.1119100, 2016b.

768 Asmi, E., Kondratyev, V., Brus, D., Laurila, T., Lihavainen, H., Backman, J., Vakkari, V.,  
769 Aurela, M., Hatakka, J., Viisanen, Y., Uttal, T., Ivakhov, V. and Makshtas, A.: Aerosol size  
770 distribution seasonal characteristics measured in Tiksi, Russian Arctic, *Atmos. Chem. Phys.*,  
771 16(3), 1271–1287, doi:10.5194/acp-16-1271-2016, 2016.

772 Barrie, L. A.: Arctic air pollution: An overview of current knowledge, *Atmos. Environ.*, 20(4),  
773 643–663, doi:10.1016/0004-6981(86)90180-0, 1986.

774 Bigg, E. K. and Leck, C.: Properties of the aerosol over the central Arctic Ocean, *J. Geophys.*  
775 *Res.*, 106(D23), 32101, doi:10.1029/1999JD901136, 2001.

776 Boé, J., Hall, A. and Qu, X.: September sea-ice cover in the Arctic Ocean projected to vanish by  
777 2100, *Nat. Geosci.*, 2(5), 341–343, doi:10.1038/ngeo467, 2009.

778 Brands, M., Kamphus, M., Böttger, T., Schneider, J., Drewnick, F., Roth, a., Curtius, J., Voigt,  
779 C., Borbon, a., Beekmann, M., Bourdon, a., Perrin, T. and Borrmann, S.: Characterization of a  
780 Newly Developed Aircraft-Based Laser Ablation Aerosol Mass Spectrometer (ALABAMA) and  
781 First Field Deployment in Urban Pollution Plumes over Paris During MEGAPOLI 2009, *Aerosol*  
782 *Sci. Technol.*, 45(1), 46–64, doi:10.1080/02786826.2010.517813, 2011.

783 Brioude, J., Arnold, D., Stohl, A., Cassiani, M., Morton, D., Seibert, P., Angevine, W., Evan, S.,

784 Dingwell, A., Fast, J. D., Easter, R. C., Pisso, I., Burkhardt, J. and Wotawa, G.: The Lagrangian  
785 particle dispersion model FLEXPART-WRF version 3.1, *Geosci. Model Dev.*, 6(6), 1889–1904,  
786 doi:10.5194/gmd-6-1889-2013, 2013.

787 Browse, J., Carslaw, K. S., Arnold, S. R., Pringle, K. and Boucher, O.: The scavenging processes  
788 controlling the seasonal cycle in Arctic sulphate and black carbon aerosol, *Atmos. Chem. Phys.*,  
789 12(15), 6775–6798, doi:10.5194/acp-12-6775-2012, 2012.

790 Browse, J., Carslaw, K. S., Mann, G. W., Birch, C. E., Arnold, S. R. and Leck, C.: The complex  
791 response of Arctic aerosol to sea-ice retreat, *Atmos. Chem. Phys.*, 14(14), 7543–7557,  
792 doi:10.5194/acp-14-7543-2014, 2014.

793 Carslaw, K. S., Lee, L. A., Reddington, C. L., Pringle, K. J., Rap, A., Forster, P. M., Mann, G.  
794 W., Spracklen, D. V., Woodhouse, M. T., Regayre, L. A. and Pierce, J. R.: Large contribution of  
795 natural aerosols to uncertainty in indirect forcing., *Nature*, 503(7474), 67–71,  
796 doi:10.1038/nature12674, 2013.

797 Chang, R. Y. W., Sjostedt, S. J., Pierce, J. R., Papakyriakou, T. N., Scarratt, M. G., Michaud, S.,  
798 Levasseur, M., Leaitch, W. R. and Abbatt, J. P. D.: Relating atmospheric and oceanic DMS  
799 levels to particle nucleation events in the Canadian Arctic, *J. Geophys. Res. Atmos.*, 116(21), 1–  
800 10, doi:10.1029/2011JD015926, 2011.

801 Charlson, R. J., Lovelock, J. E., Andreae, M. O. and Warren, S. G.: Oceanic phytoplankton,  
802 atmospheric sulphur, cloud albedo and climate, *Nature*, 326, 655–661, doi:10.1038/326655a0,  
803 1987.

804 Clarke, A. D., L, V. J., Eisele, F., Mauldin, R. L., Tanner, D. and M, L.: Particle production in  
805 the remote marine atmosphere : Cloud outflow and subsidence during ACE 1, *Earth Sci.*, 103,  
806 1998.

807 Clarke, A. D., Kapustin, V. N., Eisele, F. L., Weber, R. J. , and McMurry, P. H.: Particle  
808 production near marine clouds: sulfuric acid and predictions from classical binary nucleation,  
809 *Geophys. Res. Lett.*, 26, 2425-2428, doi: 10.1029/1999GL900438, 1999.

810 Covert, D. S., Wiedensohler, A., Aalto, P., Heintzenberg, J., McMurry, P. H. and Leck, C.:  
811 Aerosol number size distributions from 3 to 500 nm diameter in the arctic marine boundary layer

812 during summer and autumn, *Tellus, Ser. B Chem. Phys. Meteorol.*, 48(2), 197–212, 1996.

813 Croft, B., Martin, R. V., Leaitch, W. R., Tunved, P., Breider, T. J., D’Andrea, S. D. and Pierce, J.  
814 R.: Processes controlling the seasonal cycle of Arctic aerosol number and size distributions,  
815 *Atmos. Chem. Phys.*, 16, 3665-3682, doi:10.5194/acp-16-3665-2016, 2016a.

816 Croft, B., G.R. Wentworth, R.V. Martin, W.R. Leaitch, J.G. Murphy, B.N. Murphy, J. Kodros,  
817 J.P.D. Abbatt and J.R. Pierce. Contribution of Arctic seabird-colony ammonia to atmospheric  
818 particles and cloud-albedo radiative effect. *Nat. Commun.* 7, 13444, doi: 10.1038/ncomms13444,  
819 2016b.

820 DeCarlo, P. F., Kimmel, J. R., Trimborn, A., Northway, M. J., Jayne, J. T., Aiken, A. C., Gonin,  
821 M., Fuhrer, K., Horvath, T., Docherty, K. S., Worsnop, D. R. and Jimenez, J. L.: Field-  
822 deployable, high-resolution, time-of-flight aerosol mass spectrometer., *Anal. Chem.*, 78(24),  
823 8281–9, doi:10.1021/ac061249n, 2006.

824 Engvall, A.-C., Krejci, R., Ström, J., Minikin, A., Treffeisen, R., Stohl, A. and Herber, A.: In-situ  
825 airborne observations of the microphysical properties of the Arctic tropospheric aerosol during  
826 late spring and summer, *Tellus B*, 0(0), 080414161623888–???, doi:10.1111/j.1600-  
827 0889.2008.00348.x, 2008.

828 Engvall, a.-C., Krejci, R., Ström, J., Treffeisen, R., Scheele, R., Hermansen, O. and Paatero, J.:  
829 Changes in aerosol properties during spring-summer period in the Arctic troposphere, *Atmos.*  
830 *Chem. Phys.*, 8, 445-462, doi:10.5194/acp-8-445-2008, 2008.

831 Garrett, T. J.: Effects of varying aerosol regimes on low-level Arctic stratus, *Geophys. Res. Lett.*,  
832 31(17), L17105, doi:10.1029/2004GL019928, 2004.

833 Garrett, T. J., Hobbs, P. V and Radke, L. F.: High Aitken Nucleus Concentrations above Cloud  
834 Tops in the Arctic, *J. Atmos. Sci.*, 59(3), 779–783, doi:10.1175/1520-  
835 0469(2001)059<0779:HANCAC>2.0.CO;2, 2002.

836 Garrett, T. J., Brattström, S., Sharma, S., Worthy, D. E. J. and Novelli, P.: The role of  
837 scavenging in the seasonal transport of black carbon and sulfate to the Arctic, *Geophys. Res.*  
838 *Lett.*, 38(16), 1–6, doi:10.1029/2011GL048221, 2011.

839 Ge, X., Wexler, A. S. and Clegg, S. L.: Atmospheric amines - Part I. A review, *Atmos. Environ.*,  
840 45(3), 524–546, doi:10.1016/j.atmosenv.2010.10.012, 2011.

841 Gibb, S. W., Mantoura, R. F. C. and Liss, P. S.: Ocean-atmosphere exchange and atmospheric  
842 speciation of ammonia and methylamines in the region of the NW Arabian Sea, *Global*  
843 *Biogeochem. Cycles*, 13(1), 161–178, doi:10.1029/98GB00743, 1999.

844 Hegg, D. A., Radke, L. F. and Hobbs, P. V.: Particle production associated with marine clouds, *J.*  
845 *Geophys. Res. Atmos.*, 95(D9), 13917–13926, 1990.

846 Heintzenberg, B. J.: Particle size distribution and optical properties, *Tellus*, 32, 251–260,  
847 10.1111/j.2153-3490.1980.tb00952.x, 1980.

848 Heintzenberg, B., Ström, J., Ogren, J. A., and Fimpel, H.-P.: Vertical profiles of aerosol  
849 properties in the summer troposphere of central Europe, scandinavia and the svalbard region,  
850 *Atmos. Env.*, 25, 621-627, doi: 10.1016/0960-1686(91)90059-G, 1991.

851 Heintzenberg, B., and Leck, C.: Seasonal variation of the atmospheric aerosol near the top of the  
852 marine boundary layer over Spitsbergen related to the Arctic sulphur cycle. *Tellus B*, 46, 52-67,  
853 doi: 10.1034/j.1600-0889.1994.00005.x, 1994.

854 Heintzenberg, J., Leck, C., Birmili, W., Wehner, B., Tjernström, M., Wiedensohler, A.,  
855 Tjernstrom, M. and Wiedensohler, A.: Aerosol number-size distributions during clear and fog  
856 periods in the summer high Arctic: 1991, 1996 and 2001, *Tellus B*, 58(1), 41–50,  
857 doi:10.1111/j.1600-0889.2005.00171.x, 2006.

858 Heintzenberg, J. and Leck, C.: The summer aerosol in the central Arctic 1991–2008: did it  
859 change or not?, *Atmos. Chem. Phys.*, 12(9), 3969–3983, doi:10.5194/acp-12-3969-2012, 2012.

860 Heintzenberg, J., Leck, C. and Tunved, P.: Potential source regions and processes of aerosol in  
861 the summer Arctic, *Atmos. Chem. Phys.*, 15(11), 6487–6502, doi:10.5194/acp-15-6487-2015,  
862 2015.

863 Hoppel, W. a., Frick, G. M., Fitzgerald, J. W. and Larson, R. E.: Marine boundary layer  
864 measurements of new particle formation and the effects nonprecipitating clouds have on aerosol  
865 size distribution, *J. Geophys. Res.*, 99(D7), 14443, doi:10.1029/94JD00797, 1994.

866 Karl, M., Leck, C., Gross, A. and Pirjola, L.: A study of new particle formation in the marine  
867 boundary layer over the central Arctic Ocean using a flexible multicomponent aerosol dynamic  
868 model, *Tellus B*, 64(0), 1–24, doi:10.3402/tellusb.v64i0.17158, 2012.

869 Karl, M., Leck, C., Coz, E. and Heintzenberg, J.: Marine nanogels as a source of atmospheric  
870 nanoparticles in the high Arctic, *Geophys. Res. Lett.*, 40(14), 3738–3743, doi:10.1002/grl.50661,  
871 2013.

872 Kulmala, M., Dal Maso, M., Mäkelä, J. M., Pirjola, L., Väkevä, M., Aalto, P., Miikkulainen, P.,  
873 Hämeri, K. and O’Dowd, C. D.: On the formation, growth and composition of nucleation mode  
874 particles, *Tellus, Ser. B Chem. Phys. Meteorol.*, 53, 479–490, doi:10.1034/j.1600-  
875 0889.2001.d01-33.x, 2001.

876 Kupiszewski, P., Leck, C., Tjernström, M., Sjogren, S., Sedlar, J., Graus, M., Müller, M.,  
877 Brooks, B., Swietlicki, E., Norris, S. and Hansel, A.: Vertical profiling of aerosol particles and  
878 trace gases over the central Arctic Ocean during summer, *Atmos. Chem. Phys.*, 13(24), 12405–  
879 12431, doi:10.5194/acp-13-12405-2013, 2013.

880 Law, K. S., Stohl, A., Quinn, P. K., Brock, C. A., Burkhart, J. F., Paris, J. D., Ancellet, G.,  
881 Singh, H. B., Roiger, A., Schlager, H., Dibb, J., Jacob, D. J., Arnold, S. R., Pelon, J. and  
882 Thomas, J. L.: Arctic air pollution: New insights from POLARCAT-IPY, *Bull. Am. Meteorol.*  
883 *Soc.*, 95(12), 1873–1895, doi:10.1175/BAMS-D-13-00017.1, 2014.

884 Leaitch, W.R., Hoff, R.M., Melnichuk, S., and Hogan, W.: Some chemical and physical  
885 properties of the Arctic winter aerosol in northeastern Canada. *J. Climate Appl. Meteorol.*, 23,  
886 916-928, [http://dx.doi.org/10.1175/1520-0450\(1984\)023<0916:SPACPO>2.0.CO;2](http://dx.doi.org/10.1175/1520-0450(1984)023<0916:SPACPO>2.0.CO;2), 1984.

887 Leaitch, W.R., Barrie, L.A., Bottenheim, J.W., Li, S.-M., Shepson, P. and Yokouchi, Y.:  
888 Airborne observations related ozone depletion at polar sunrise. *J. Geophys. Res.*, 99, 25499-  
889 25517, 10.1029/94JD02750, 1994.

890 Leaitch, W. R., Sharma, S., Huang, L., Toom-Saunty, D., Chivulescu, A., Macdonald, A. M.,  
891 von Salzen, K., Pierce, J. R., Bertram, A. K., Schroder, J. C., Shantz, N. C., Chang, R. Y. W. and  
892 Norman, A.-L.: Dimethyl sulfide control of the clean summertime Arctic aerosol and cloud,  
893 *Elem. Sci. Anth.*, 1(1), 17, doi:10.12952/journal.elementa.000017, 2013.



894 Leaitch, W. R., Korolev, A., Aliabadi, A. A., Burkart, J., Willis, M., Abbatt, J. P. D., Bozem, H.,  
895 Hoor, P., Köllner, F., Schneider, J., Herber, A., Konrad, C. and Brauner, R.: Effects of 20-100  
896 nanometre particles on liquid clouds in the clean summertime Arctic, *Atmos. Chem. Phys.*, 16,  
897 11107-11124, doi:10.5194/acp-16-11107-2016, 2016.

898 Leck, C. and Bigg, E. K.: Aerosol production over remote marine areas-A new route, *Geophys.*  
899 *Res. Lett.*, 26(23), 3577, doi:10.1029/1999GL010807, 1999.

900 Leck, C. and Bigg, E. K.: Source and evolution of the marine aerosol - A new perspective,  
901 *Geophys. Res. Lett.*, 32(19), 1–4, doi:10.1029/2005GL023651, 2005.

902 Leck, C. and Bigg, E. K.: New Particle Formation of Marine Biological Origin, *Aerosol Sci.*  
903 *Technol.*, 44(7), 570–577, doi:10.1080/02786826.2010.481222, 2010.

904 Lohmann, U. and Feichter, J.: Global indirect aerosol effects: a review, *Atmos. Chem. Phys.*, 5,  
905 715–735, doi:10.5194/acp-5-715-2005, 2005.

906 Mauldin, R. L., Madronich, S., Flocke, S. J. , Eisele, F. L. , Frost, G. J. and Prevot, A. S. H. :  
907 New insights on OH: Measurements around and in clouds, *Geophys. Res. Lett.*, 24(No 23),  
908 3033-3036, doi:10.1029/97GL02983, 1997.

909 Mauritsen, T., Sedlar, J., Tjernström, M., Leck, C., Martin, M., Shupe, M., Sjogren, S., Sierau,  
910 B., Persson, P. O. G., Brooks, I. M. and Swietlicki, E.: An Arctic CCN-limited cloud-aerosol  
911 regime, *Atmos. Chem. Phys.*, 11(1), 165–173, doi:10.5194/acp-11-165-2011, 2011.

912 Mungall, E. L., Croft, B., Lizotte, M., Thomas, J. L., Murphy, J. G., Levasseur, M., Martin, R.  
913 V., Wentzell, J. J. B., Liggio, J. and Abbatt, J. P. D.: Dimethyl sulfide in the summertime Arctic  
914 atmosphere: measurements and source sensitivity simulations, *Atmos. Chem. Phys.*, 16(11),  
915 6665–6680, doi:10.5194/acp-16-6665-2016, 2016.

916 Nguyen, Q. T., Glasius, M., Sørensen, L. L., Jensen, B., Skov, H., Birmili, W., Wiedensohler, A.,  
917 Kristensson, A., Nøjgaard, J. K. and Massling, A.: Seasonal variation of atmospheric particle  
918 number concentrations, new particle formation and atmospheric oxidation capacity at the high  
919 Arctic site Villum Research Station, Station Nord, *Atmos. Chem. Phys. Discuss.*, 1–41,  
920 doi:10.5194/acp-2016-205, 2016.

921 Petters, M. D. and Kreidenweis, S. M.: A single parameter representation of hygroscopic growth  
922 and cloud condensation nucleus activity, *Atmos. Chem. Phys.*, 7, 1961–1971, 2007.

923 Pierce, J. R., Leaitch, W. R., Liggitto, J., Westervelt, D. M., Wainwright, C. D., Abbatt, J. P. D.,  
924 Ahlm, L., Al-Basheer, W., Cziczo, D. J., Hayden, K. L., Lee, A. K. Y., Li, S.-M., Russell, L. M.,  
925 Sjostedt, S. J., Strawbridge, K. B., Travis, M., Vlasenko, A., Wentzell, J. J. B., Wiebe, H. A.,  
926 Wong, J. P. S., and Macdonald, A. M.: Nucleation and condensational growth to CCN sizes  
927 during a sustained pristine biogenic SOA event in a forested mountain valley, *Atmos. Chem.*  
928 *Phys.*, 12, 3147-3163, doi:10.5194/acp-12-3147-2012, 2012.

929 Pirjola, L., O'Dowd, C. D., Brooks, I. M. and Kulmala, M.: Can new particle formation occur in  
930 the clean marine boundary layer?, *J. Geophys. Res. Atmos.*, 105(D21), 26531–26546,  
931 doi:10.1029/2000JD900310, 2000.

932 Quinn, P. K. and Bates, T. S.: The case against climate regulation via oceanic phytoplankton  
933 sulphur emissions, *Nature*, 480(7375), 51–56, doi:10.1038/nature10580, 2011.

934 Quinn, P. K., Shaw, G., Andrews, E., Dutton, E. G., Ruoho-Airola, T. and Gong, S. L.: Arctic  
935 haze: Current trends and knowledge gaps, *Tellus, Ser. B Chem. Phys. Meteorol.*, 59(1), 99–114,  
936 doi:10.1111/j.1600-0889.2006.00238.x, 2007.

937 Radke, F. L. and Hobbs, P. V.: Humidity and particle fields around some small cumulus clouds,  
938 *Journal of atmospheric sciences*, 48(9), 1190-1193, doi: [http://dx.doi.org/10.1175/1520-](http://dx.doi.org/10.1175/1520-0469(1991)048<1190:HAPFAS>2.0.CO;2)  
939 [0469\(1991\)048<1190:HAPFAS>2.0.CO;2](http://dx.doi.org/10.1175/1520-0469(1991)048<1190:HAPFAS>2.0.CO;2), 1991.

940 Rahn, K. A., Borys, R. D. and Shaw, G. E.: The Asian source of Arctic haze bands, *Nature*, 268,  
941 713-715, doi: 10.1038/268713a0, 1977.

942 Rehbein, P. J. G., Jeong, C. H., McGuire, M. L., Yao, X., Corbin, J. C. and Evans, G. J.: Cloud  
943 and fog processing enhanced gas-to-particle partitioning of trimethylamine, *Environ. Sci.*  
944 *Technol.*, 45(10), 4346–4352, doi:10.1021/es1042113, 2011.

945 Riipinen, I., Pierce, J. R., Yli-Juuti, T., Nieminen, T., Häkkinen, S., Ehn, M., Junninen, H.,  
946 Lehtipalo, K., Petäjä, T., Slowik, J., Chang, R., Shantz, N. C., Abbatt, J., Leaitch, W. R.,  
947 Kerminen, V.-M., Worsnop, D. R., Pandis, S. N., Donahue, N. M., and Kulmala, M.: Organic

948 condensation: a vital link connecting aerosol formation to cloud condensation nuclei (CCN)  
949 concentrations, *Atmos. Chem. Phys.*, 11, 3865-3878, doi:10.5194/acp-11-3865-2011, 2011.

950 Seinfeld, J.H., and Pandis, S. N.: *Atmospheric Chemistry and Physics: From Air Pollution to*  
951 *Climate Change*. 3rd Edition. John Wiley & Sons, Inc., 2016.

952 Shaw, G.E. and Stamnes, K.: Arctic haze: perturbations of the polar radiation budget. *Ann. N. E*  
953 *Ad. Aci.* 338, 533-539, doi: 10.1111/j.1749-6632.1980.tb17145.x 1980.

954

955 Shaw, G. E.: The Arctic Haze Phenomenon, *Bull. Am. Meteorol. Soc.*, 76, 2403–2413,  
956 doi:10.1175/1520-0477(1995)076<2403:TAHP>2.0.CO;2, 1995.

957 Skamarock, W. C., Klemp, J. B., Dudhia, J., Gill, D. O., Barker, D. M., Wang, W. and Powers, J.  
958 G.: A Description of the Advanced Research WRF Version 2, [online] Available from:  
959 <http://oai.dtic.mil/oai/oai?verb=getRecord&metadataPrefix=html&identifier=ADA487419>  
960 (Accessed 22 March 2016), 2005.

961 Sjostedt, S. J., Leaitch, W. R., Levasseur, M., Scarratt, M., Michaud, S., Motard-Côté, J.,  
962 Burkhardt, J. H., and Abbatt J.: Evidence for the uptake of atmospheric acetone and methanol by  
963 the Arctic Ocean during late summer DMS-Emission plumes. *J. Geophys. Res.*, 117, D12303,  
964 doi: 10.1029/2011JD017086, 2012.

965 Stohl, a., Forster, C., Frank, A., Seibert, P. and Wotawa, G.: Technical note: The Lagrangian  
966 particle dispersion model FLEXPART version 6.2, *Atmos. Chem. Phys. Discuss.*, 5(4), 4739–  
967 4799, doi:10.5194/acpd-5-4739-2005, 2005.

968 Ström, J., Umegård, J., Tørseth, K., Tunved, P., Hansson, H. C., Holmén, K., Wismann, V.,  
969 Herber, A. and König-Langlo, G.: One year of particle size distribution and aerosol chemical  
970 composition measurements at the Zeppelin Station, Svalbard, March 2000-March 2001, *Phys.*  
971 *Chem. Earth*, 28(March 2000), 1181–1190, doi:10.1016/j.pce.2003.08.058, 2003.

972 Ström, J., Engvall, A. C., Delbart, F., Krejci, R. and Treffeisen, R.: On small particles in the  
973 Arctic summer boundary layer: Observations at two different heights near Ny-Ålesund,  
974 Svalbard, *Tellus, Ser. B Chem. Phys. Meteorol.*, 61 B(2), 473–482, doi:10.1111/j.1600-

975 0889.2008.00412.x, 2009.

976 Tjernström, M., Birch, C. E., Brooks, I. M., Shupe, M. D., Persson, P. O. G., Sedlar, J.,  
977 Mauritsen, T., Leck, C., Paatero, J., Szczodrak, M. and Wheeler, C. R.: Meteorological  
978 conditions in the central Arctic summer during the Arctic Summer Cloud Ocean Study  
979 (ASCOS), *Atmos. Chem. Phys.*, 12(15), 6863–6889, doi:10.5194/acp-12-6863-2012, 2012.

980 Tjernström, M., Leck, C., Birch, C. E., Bottenheim, J. W., Brooks, B. J., Brooks, I. M., Bäcklin,  
981 L., Chang, R. Y. W., De Leeuw, G., Di Liberto, L., De La Rosa, S., Granath, E., Graus, M.,  
982 Hansel, a., Heintzenberg, J., Held, a., Hind, a., Johnston, P., Knulst, J., Martin, M., Matrai, P.  
983 a., Mauritsen, T., Müller, M., Norris, S. J., Orellana, M. V., Orsini, D. a., Paatero, J., Persson, P.  
984 O. G., Gao, Q., Rauschenberg, C., Ristovski, Z., Sedlar, J., Shupe, M. D., Sierau, B., Sirevaag,  
985 a., Sjogren, S., Stetzer, O., Swietlicki, E., Szczodrak, M., Vaattovaara, P., Wahlberg, N.,  
986 Westberg, M. and Wheeler, C. R.: The Arctic Summer Cloud Ocean Study (ASCOS): Overview  
987 and experimental design, *Atmos. Chem. Phys.*, 14(6), 2823–2869, doi:10.5194/acp-14-2823-  
988 2014, 2014.

989 Tunved, P., Ström, J. and Krejci, R.: Arctic aerosol life cycle: linking aerosol size distributions  
990 observed between 2000 and 2010 with air mass transport and precipitation at Zeppelin station,  
991 Ny-Ålesund, Svalbard, *Atmos. Chem. Phys.*, 13(7), 3643–3660, doi:10.5194/acp-13-3643-2013,  
992 2013.

993 Twomey, S.: Pollution and the Planetary Albedo, *Atmos. Environ.*, 41(Vol. 8), 1251–1256,  
994 doi:10.1016/j.atmosenv.2007.10.062, 1974.

995 Wang, M. and Overland, J. E.: A sea ice free summer Arctic within 30 years: An update from  
996 CMIP5 models, *Geophys. Res. Lett.*, 39(17), 2–6, doi:10.1029/2012GL052868, 2012.

997 Weber, R. J., McMurry, P. H., Mauldin, L., Tanner, D. J., Eisele, F. L., Brechtel, F. J.,  
998 Kreidenweis, S. M., Kok, G. L., Schillawski, R. D. and Baumgardner, D.: A study of new  
999 particle formation and growth involving biogenic and trace gas species measured during ACE 1,  
1000 *J. Geophys. Res.*, 103(D13), 16385–16396, doi:10.1029/97JD02465, 1998.

1001 Wentworth, G. R., Murphy, J. G., Croft, B., Martin, R. V., Pierce, J. R., Côté, J.-S., Courchesne,  
1002 I., Tremblay, J.-É., Gagnon, J., Thomas, J. L., Sharma, S., Toom-Sauntry, D., Chivulescu, a.,

1003 Levasseur, M. and Abbatt, J. P. D.: Ammonia in the summertime Arctic marine boundary layer:  
1004 sources, sinks and implications, *Atmos. Chem. Phys.*, 16, 1937-1953, doi:10.5194/acp-16-1937-  
1005 2016, 2016.

1006 Wiedensohler, A., Covert, D. S., Swietlicki, E., Aalto, P., Heintzenberg, J. and Leck, C.:  
1007 Occurrence of an ultrafine particle mode less than 20 nm in diameter in the marine boundary  
1008 layer during Arctic summer and autumn, *Tellus, Ser. B Chem. Phys. Meteorol.*, 48(2), 213–222,  
1009 doi:10.1034/j.1600-0889.1996.t01-1-00006.x, 1996.

1010 Wiedensohler, A. H.-C. Hansson, D. Orsini, M. Wendisch, F. Wagner, K.N. Bower, T.W.  
1011 Chourlarton, M. Wells, M. Parkin, K. Acker, W. Wieprecht, M.C. Facchini, J.A. Lind, S. Fuzzi,  
1012 B.G. Arends, M. Kulmalao: Night-time formation and occurrence of new particles associated  
1013 with orographic clouds, *Atmos. Env.*, 31(16), 2445-2559, doi: [http://dx.doi.org/10.1016/S1352-](http://dx.doi.org/10.1016/S1352-2310(96)00299-3)  
1014 [2310\(96\)00299-3](http://dx.doi.org/10.1016/S1352-2310(96)00299-3), 1997.

1015 Willis, M. D., Burkart, J., Thomas, J. L., Köllner, F., Schneider, J., Bozem, H., Hoor, P. M.,  
1016 Aliabadi, A. A., Schulz, H., Herber, A. B., Leaitch, W. R. and Abbatt, J. P. D.: Growth of  
1017 nucleation mode particles in the summertime Arctic: a case study, *Atmos. Chem. Phys.*, 7663–  
1018 7679, doi:10.5194/acp-16-7663-2016, 2016.

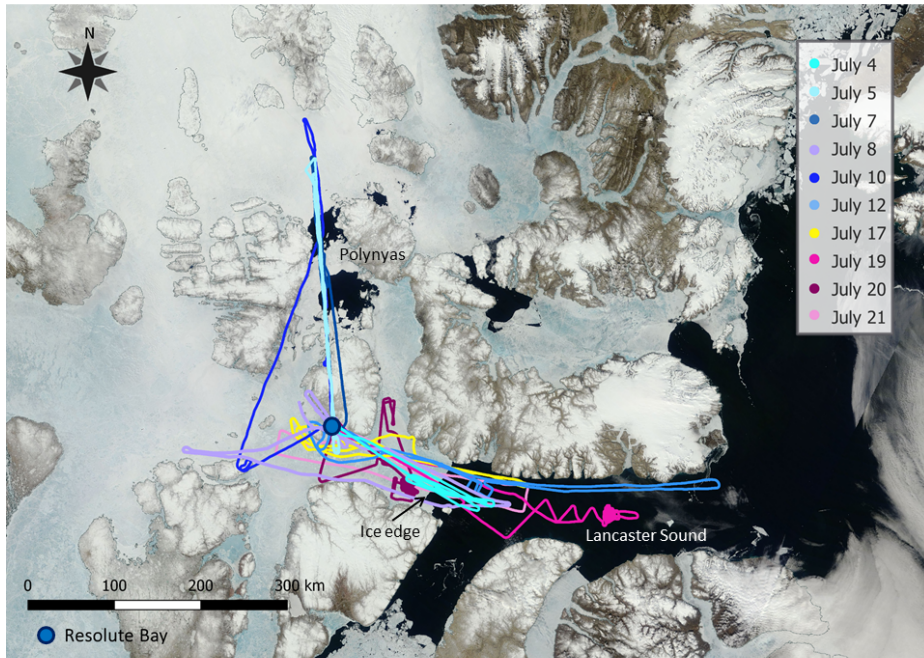
1019 Zhang, J., Spitz, Y. H., Steele, M., Ashjian, C., Campbell, R., Berline, L. and Matrai, P.:  
1020 Modeling the impact of declining sea ice on the Arctic marine planktonic ecosystem, *J. Geophys.*  
1021 *Res. Ocean.*, 115(10), 1–24, doi:10.1029/2009JC005387, 2010.

1022

1023

1023

1024

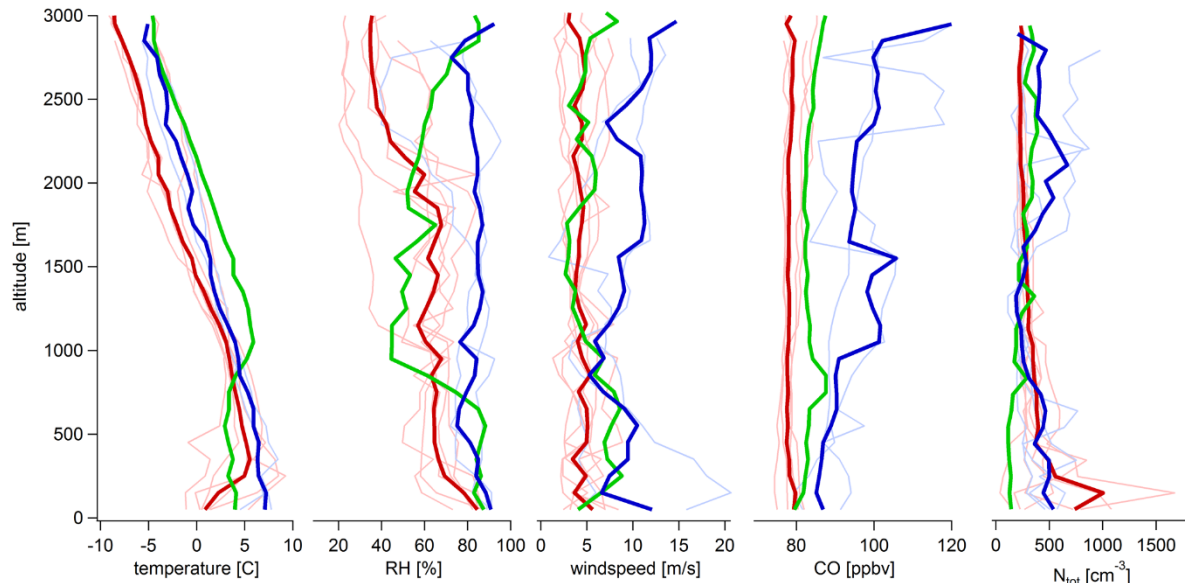


1025

1026 Figure 1. Compilation of all flight tracks plotted on a satellite image from July 4, 2014. The  
1027 image is taken from: <https://earthdata.nasa.gov/labs/worldview>.

1028

1028



1029

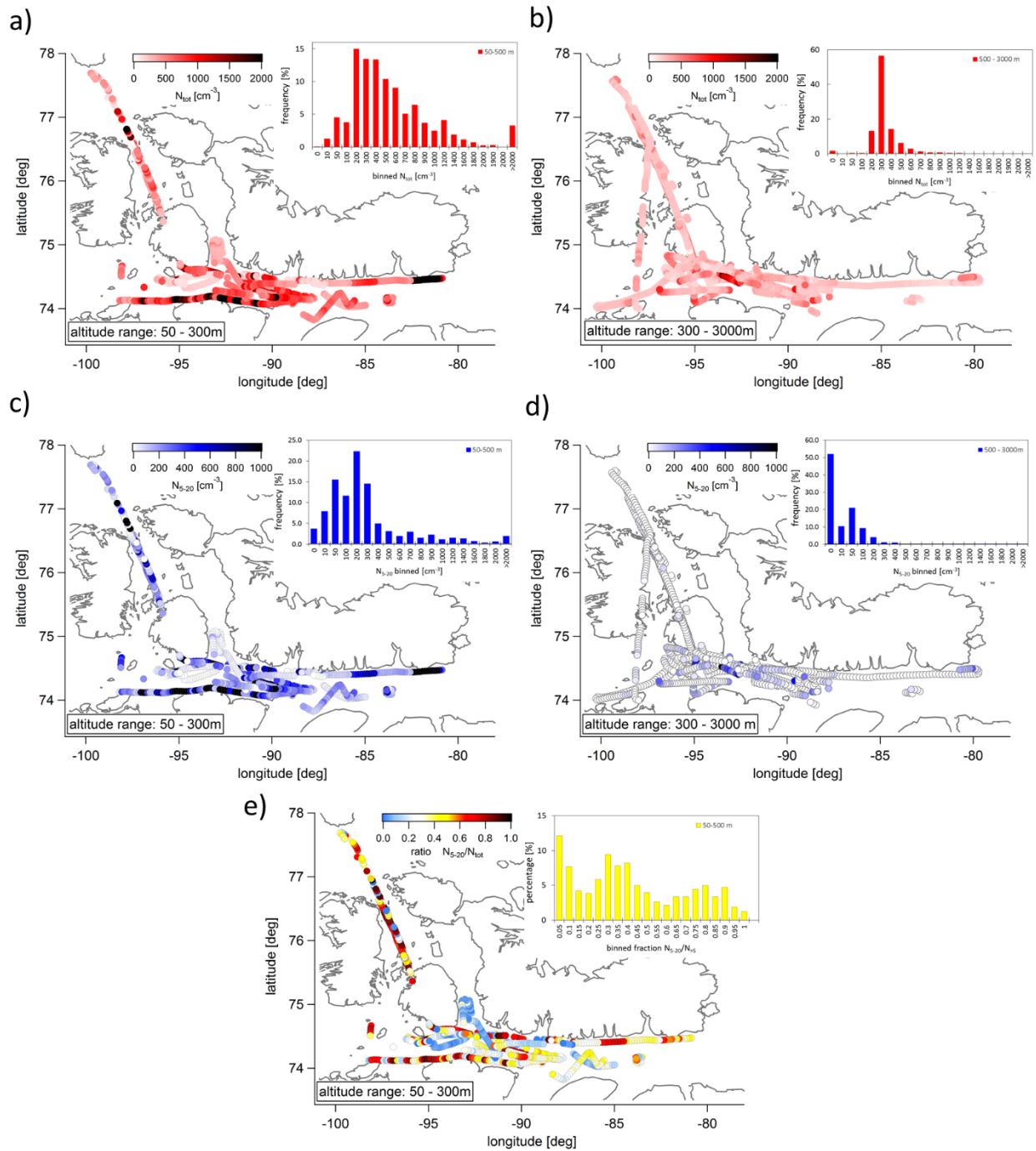
1030 Figure 2. Median temperature, relative humidity (RH), wind speed, CO mixing ratio and  $N_{\text{tot}}$   
1031 profiles for the Arctic air mass period (dark red), the transition day (dark green), and the southern  
1032 air mass period (dark blue). Median profiles for each flight are plotted in the background in the  
1033 corresponding light colours.

1034

1035

1036

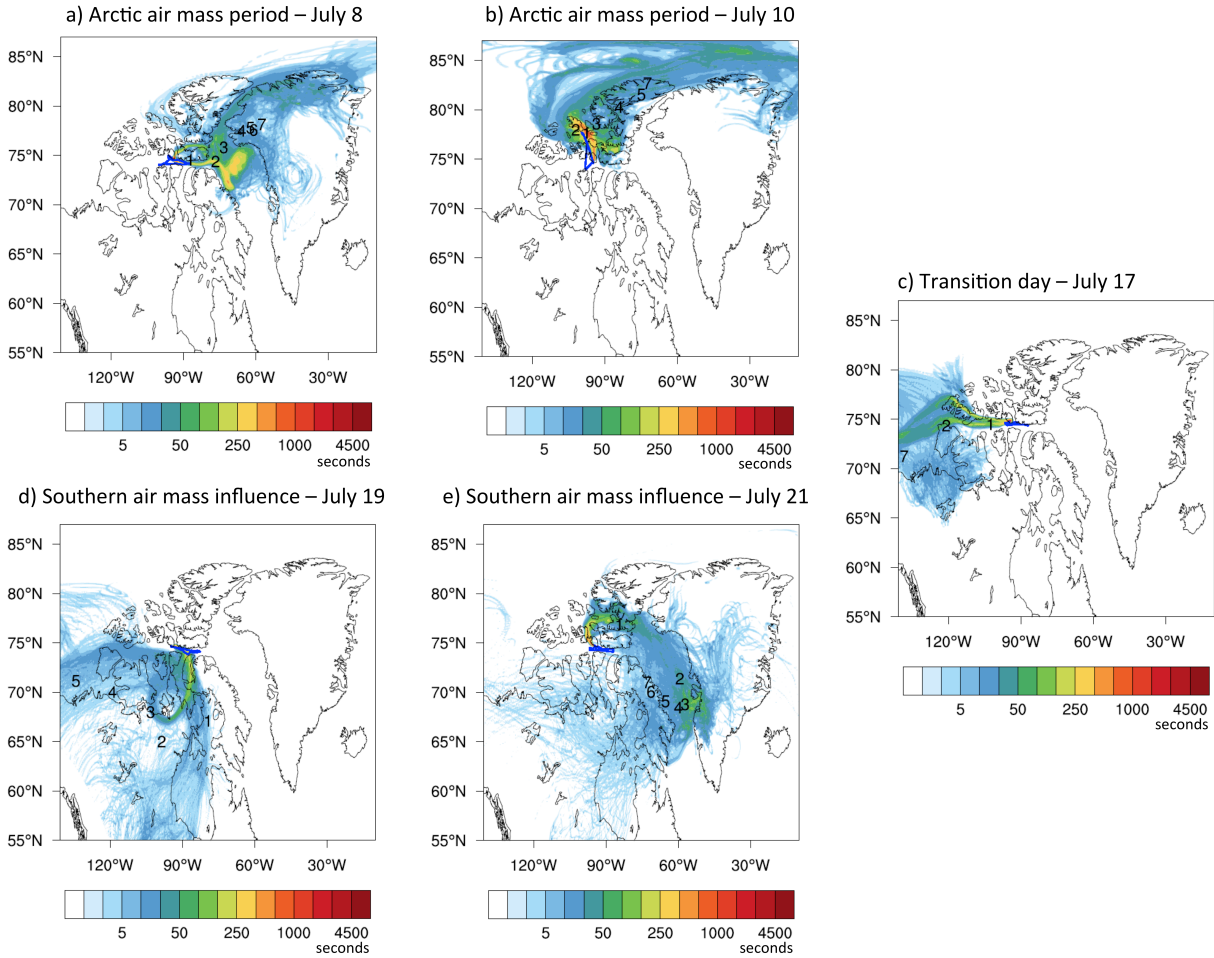
1037



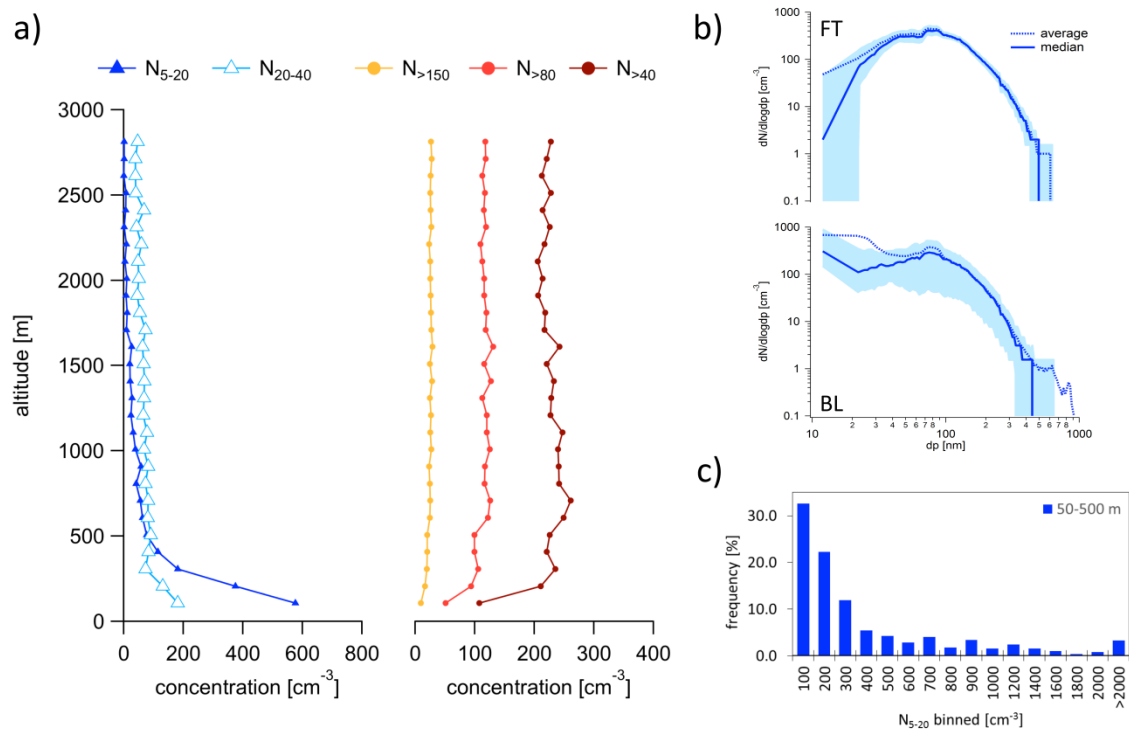
1037  
 1038 Figure 3. Flight tracks colour coded by particle concentrations. a.) Flight tracks within the  
 1039 boundary layer (50-300 m) colour coded by  $N_{tot}$ . b) Flight tracks within the free troposphere  
 1040 (300-3000 m) colour coded by  $N_{tot}$ . c) Flight tracks within the boundary layer (50-300m) colour



1041 coded by UFP. d) Flight tracks within the free troposphere (300-3000 m) colour coded by  $N_{5-20}$ .  
 1042 e) Flight tracks within the boundary layer (50-300 m) colour coded by the ratio of  $N_{5-20}/N_{tot}$   
 1043



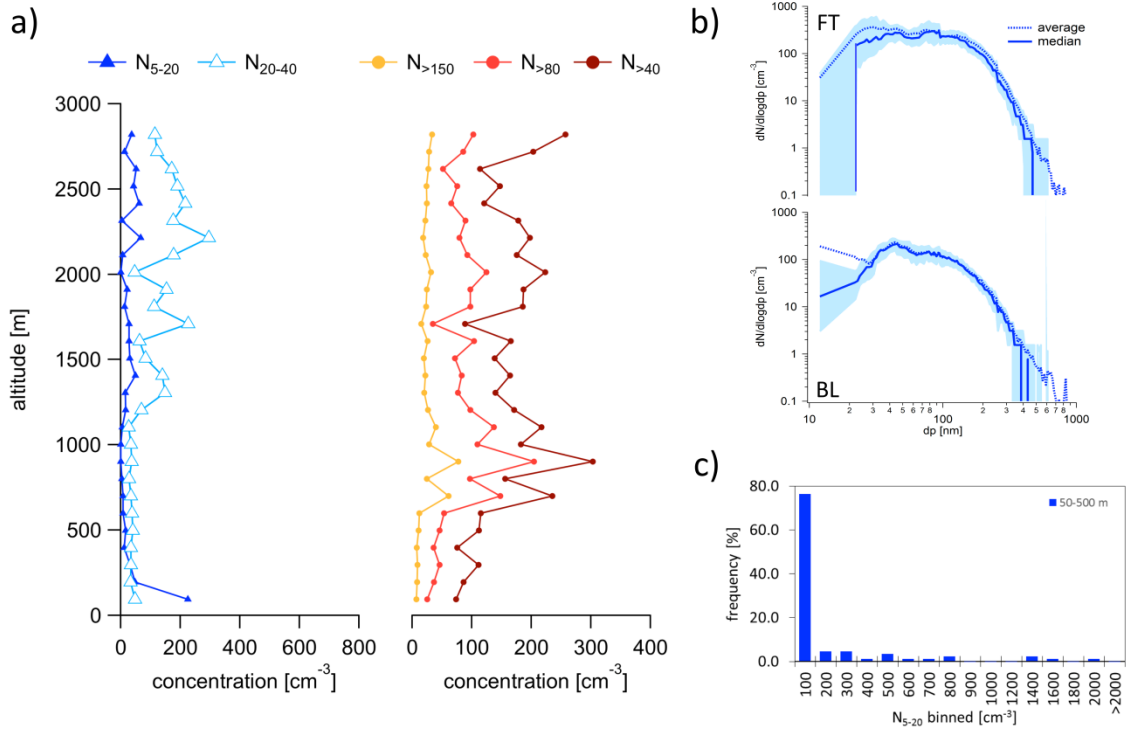
1044  
 1045 Figure 4. FLEXPART-WRF potential emissions sensitivities for each flight (using particle  
 1046 releases every 2 minutes along the flight track) that illustrate transport regimes during different  
 1047 periods of the campaign. The colour code indicates the residence time of air in seconds and the  
 1048 numbers represent the position of the plume centroid location in days prior to release (days 1-7).  
 1049



1050

1051 Figure 5. Average particle concentration data during the Arctic air mass period. a) Average  
 1052 vertical profiles of  $N_{5-20}$ ,  $N_{20-40}$ ,  $N_{40}$ ,  $N_{80}$ , and  $N_{150}$ . b) Average (solid line) and median  
 1053 (dashed line) size distribution within the BL and the FT. The light blue area represents the 25-  
 1054 75<sup>th</sup> % percentile range. c) Frequency distribution of the occurrence of UFP illustrates the large  
 1055 variability of the UFP concentrations within the BL.

1056

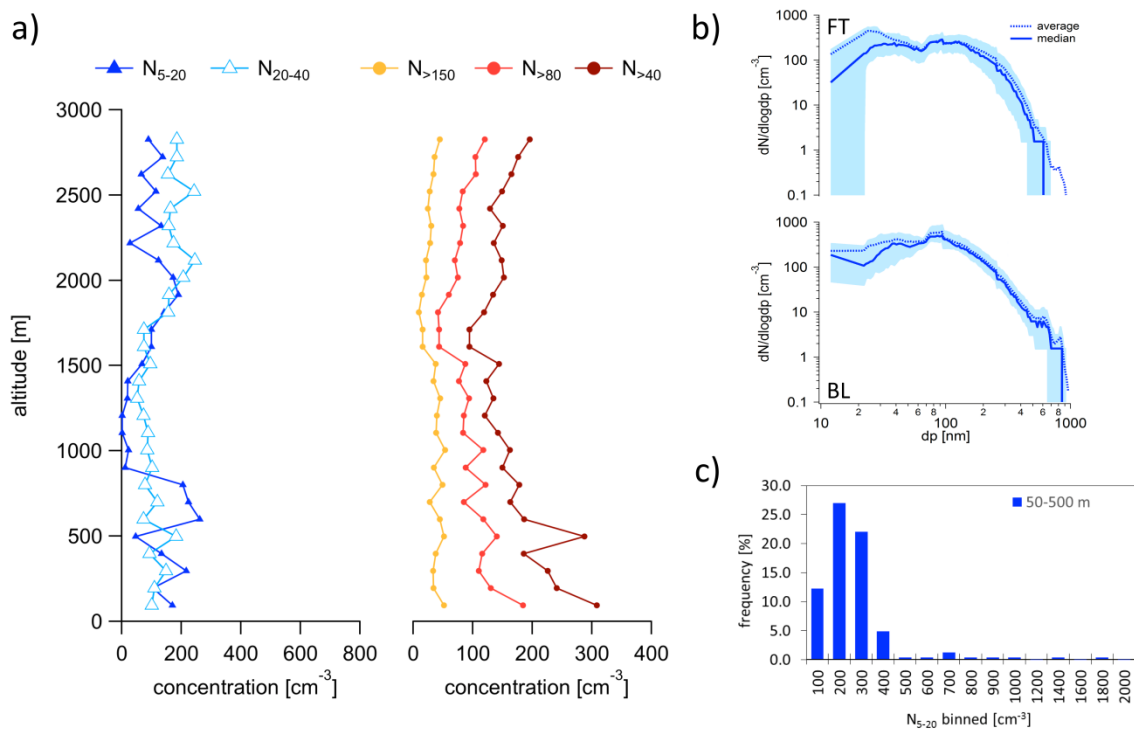


1057

1058 Figure 6. Average particle concentration data on the transition day. a) Average vertical profiles  
1059 of N<sub>5-20</sub>, N<sub>20-40</sub>, N<sub>>40</sub>, N<sub>>80</sub>, and N<sub>>150</sub>. b) Average (solid line) and median (dashed line) size  
1060 distribution within the BL and the FT. The light blue area represents the 25-75<sup>th</sup> % percentile  
1061 range. c) Frequency distribution of the occurrence of UFP illustrates the large variability of the  
1062 UFP concentrations within the BL.

1063

1063

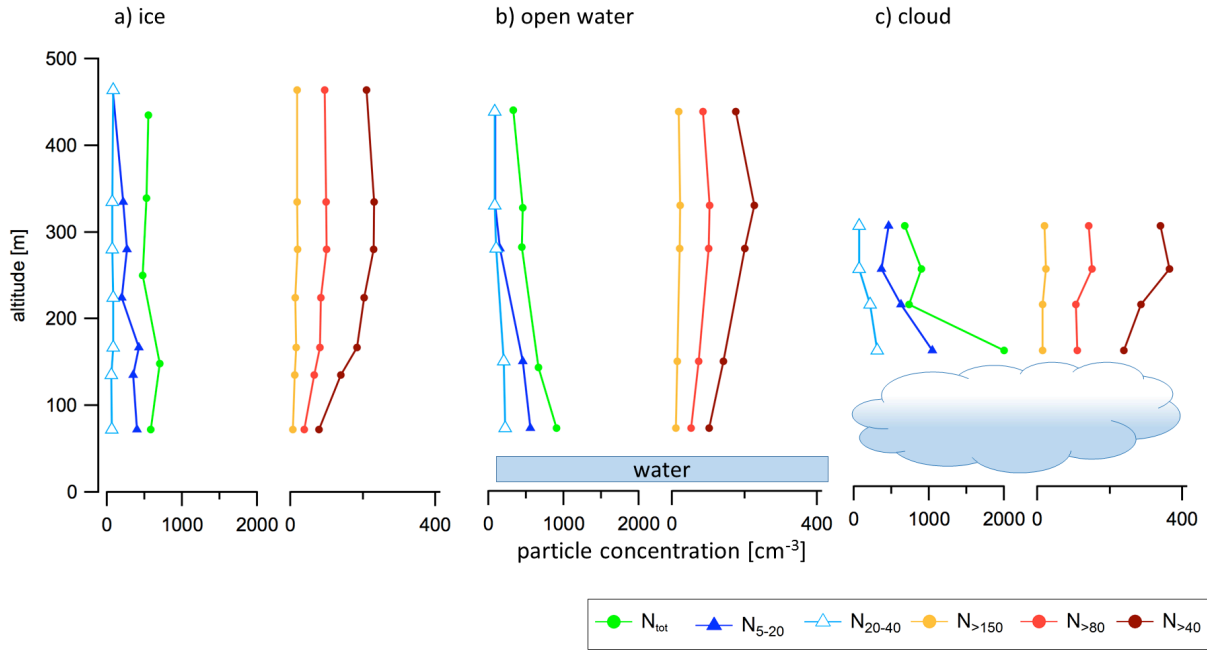


1064

1065 Figure 7. Average particle concentration data during the southern air mass period. a) Average  
 1066 vertical profiles of  $N_{5-20}$ ,  $N_{20-40}$ ,  $N_{>40}$ ,  $N_{>80}$ , and  $N_{>150}$ . b) Average (solid line) and median  
 1067 (dashed line) size distribution within the BL and the FT. The light blue area represents the 25-  
 1068 75<sup>th</sup> % percentile range. c) Frequency distribution of the occurrence of UFP illustrates the large  
 1069 variability of the UFP concentrations within the BL.

1070

1070

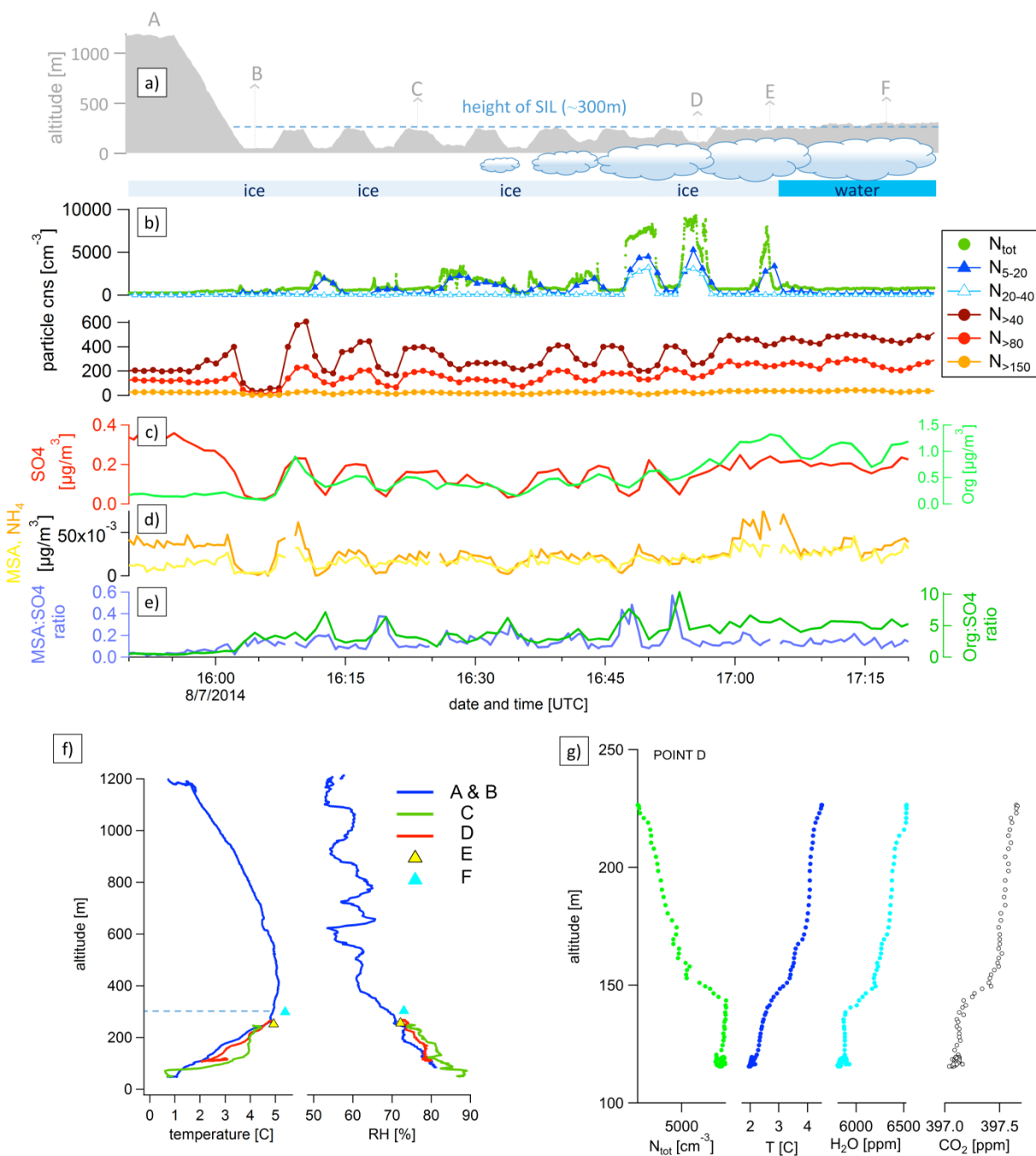


1071

1072 Figure 8. Average profiles of particle concentrations above ice, open water and cloud. The  
1073 number of data points for each specific profile is: 130 above water, 216 above cloud, and 123  
1074 above water.

1075

1076



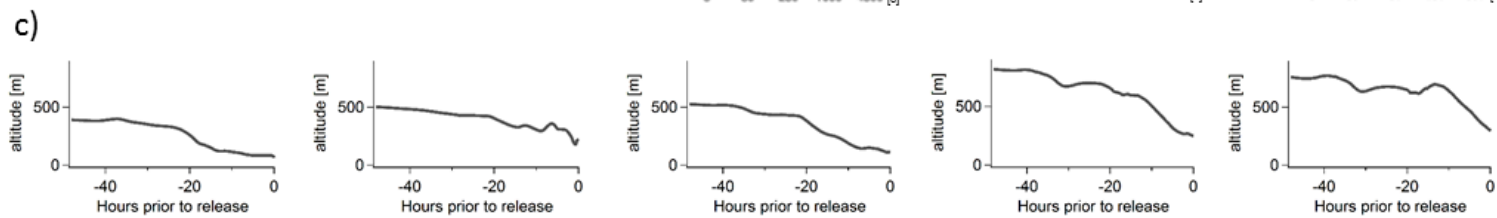
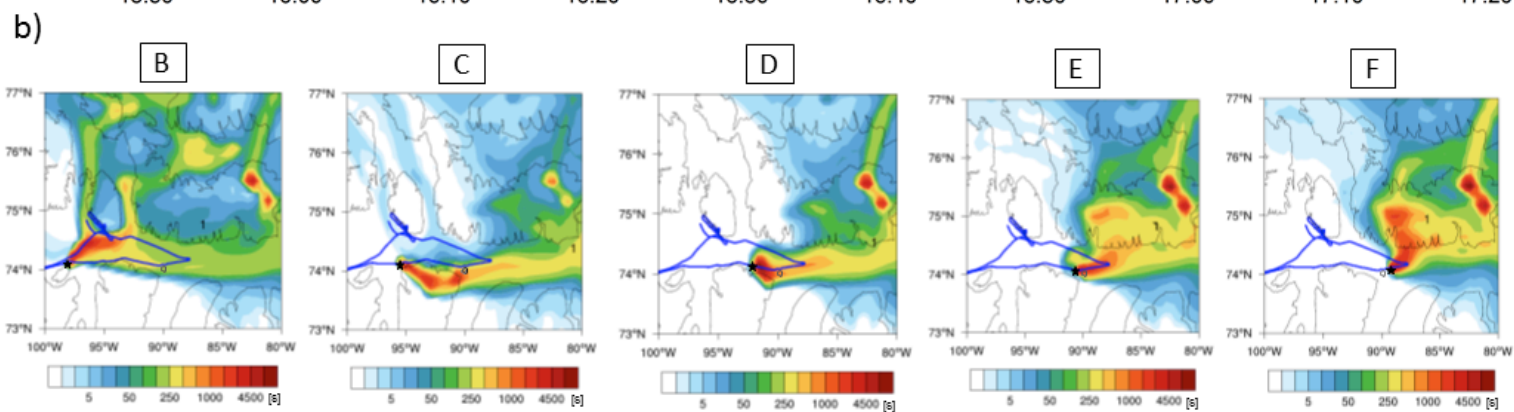
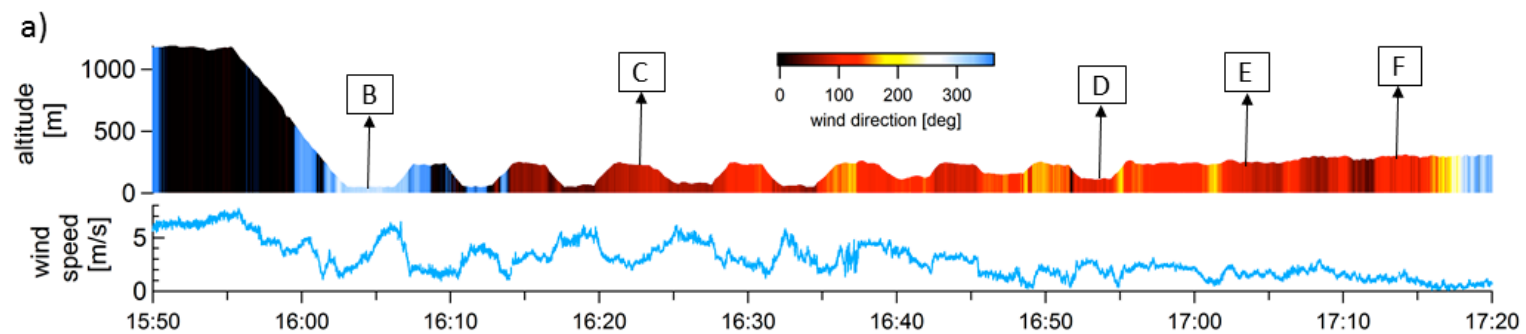
1077

1078

1079 Figure 9. Case study from July 8 flight. Time series of flight altitude and illustration of the  
 1080 surface including cloud coverage (a), aerosol size (b) and chemical composition (c-e). (f)

- 1081 Vertical profiles of temperature and RH at locations A-F. (g)  $N_{\text{tot}}$ , temperature, H<sub>2</sub>O mixing ratio  
1082 and CO<sub>2</sub> profiles at location D.

1083



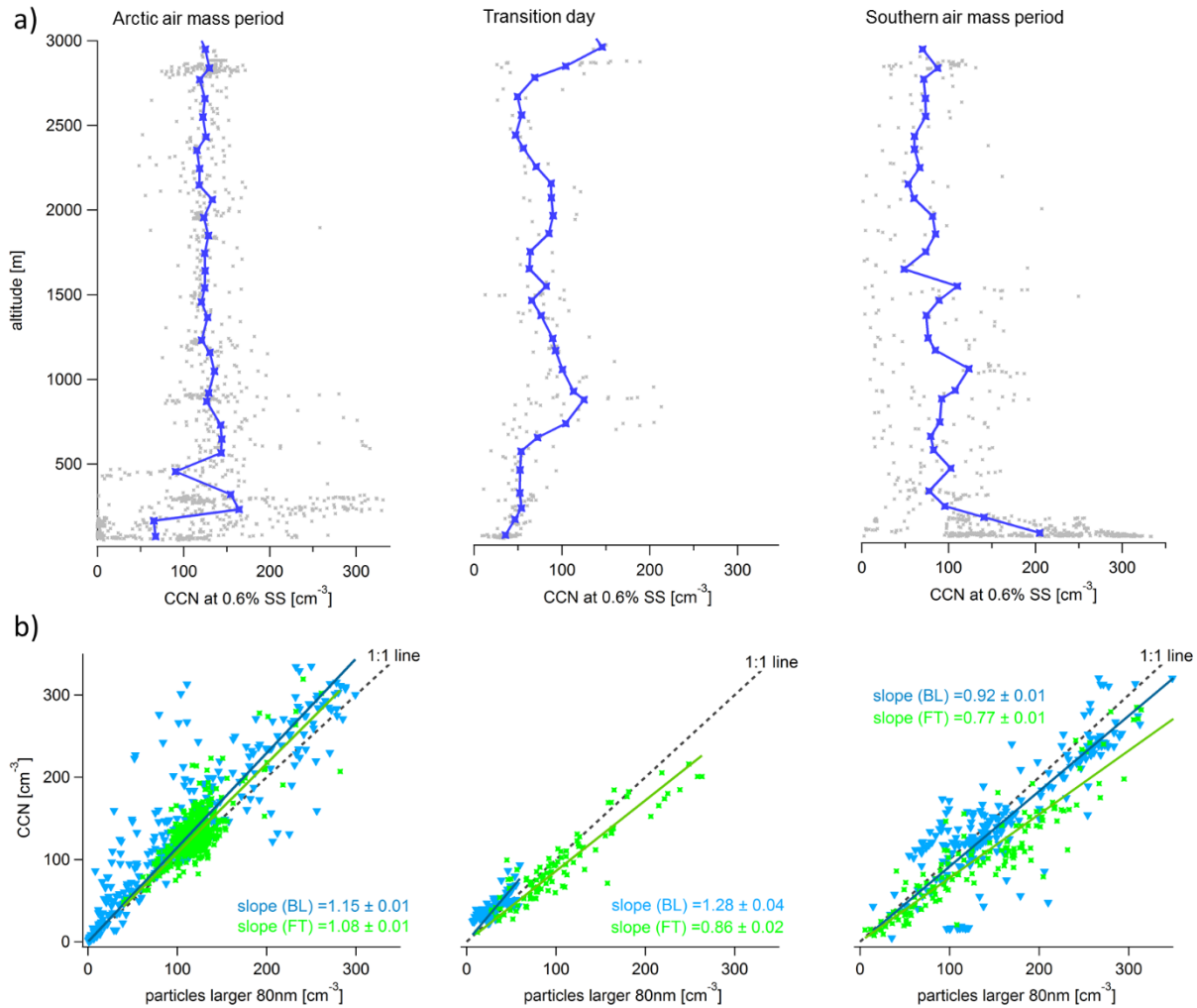
1084

1085



1086 Figure 10. (a) Time series of aircraft altitude color coded with the wind direction and time series of wind speed (b) FLEXPART-WRF  
1087 seven day backwards potential emissions sensitivities for points along the flight track (60 second release at time at indicated time and  
1088 location) showing the air mass history at 5 representative locations within the SIL. The plume centroid location for particles with age  
1089 of one day is indicated. (c) The bottom plots show the altitude of plume centroid 48 hours back in time.

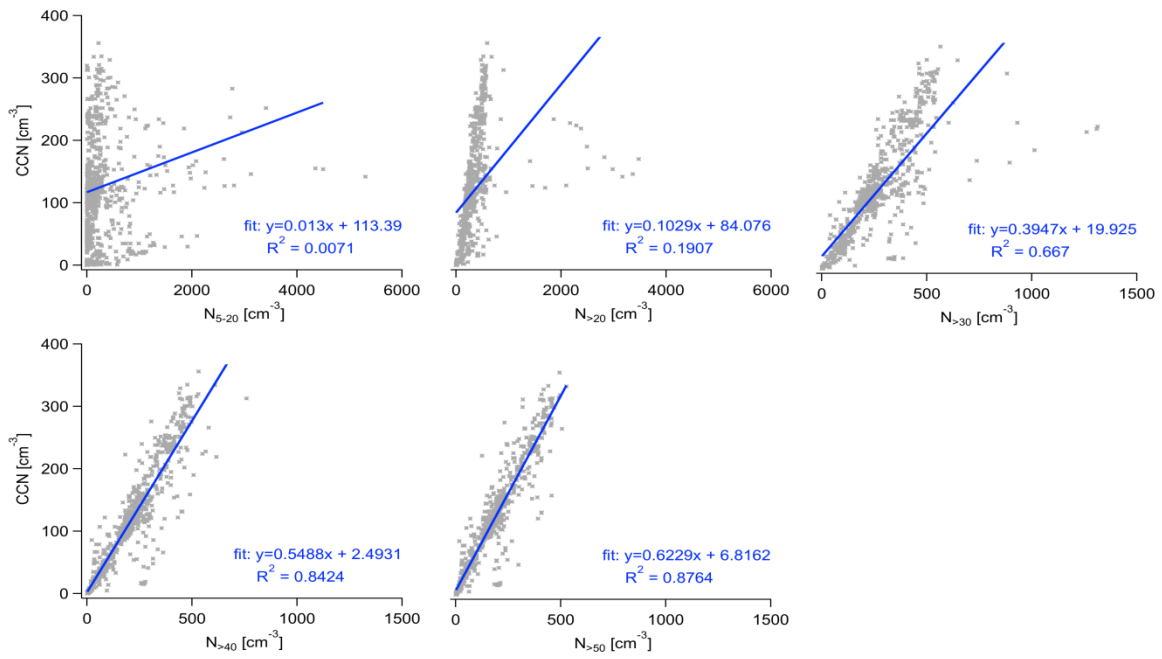
1090  
1091  
1092



1093  
1094  
1095  
1096  
1097  
1098  
1099

Figure 11. (a) Vertical profiles of average CCN concentrations (dark blue). All data points are plotted in light grey. (b) Correlation plots between CCN concentrations and particles larger than 80nm.

1099



1100

1101

1102 Figure 12. Correlations between CCN and particle concentrations for the full study period.

1103

1104

1105